NAVAL POSTGRADUATE SCHOOL
MONTEREY, CALIFORNIA

THESIS

YELLOW SEA THERMAL STRUCTURE

by

Charles R. Fralick, Jr.

September 1994

Thesis Advisor: Peter C. Chu
Co-Advisor: Steven D. Haeger

Approved for public release; distribution is unlimited.

REPORT DOCUMENTATION PAGE

Form Approved OMB No. 0704-0188

1. AGENCY USE ONLY *(Leave blank)*	2. REPORT DATE September 94	3. REPORT TYPE AND DATES COVERED Master's Thesis

4. TITLE AND SUBTITLE YELLOW SEA THERMAL STRUCTURE (U)

5. FUNDING NUMBERS

6. AUTHOR(S) Charles R. Fralick, Jr.

7. PERFORMING ORGANIZATION NAME(S) AND ADDRESS(ES)
Naval Postgraduate School
Monterey CA 93943-5000

8. PERFORMING ORGANIZATION REPORT NUMBER

9. SPONSORING/MONITORING AGENCY NAME(S) AND ADDRESS(ES)
U.S. Naval Oceanographic Office
Stennis Space Center, MS 39522

10. SPONSORING/MONITORING AGENCY REPORT NUMBER

11. SUPPLEMENTARY NOTES The views expressed in this thesis are those of the author and do not reflect the official policy or position of the Department of Defense or the U.S. Government.

12a. DISTRIBUTION/AVAILABILITY STATEMENT
Approved for public release; distribution is unlimited.

12b. DISTRIBUTION CODE

13. ABSTRACT *(maximum 200 words)* There exists a need in the oceanography community to be able to produce climatologies of remote or poorly sampled shallow water areas through remote sensing techniques. Our goal was to construct a three-dimensional thermal structure of the Yellow Sea based primarily upon sea surface temperature data. The ability to do this successfully could lead the way to applying these techniques elsewhere using remotely sensed SST. The shallow water and dynamic conditions of the Yellow Sea made it an ideal study area. The large MOODS observational data set for the area provided us with 15,000 observations from 1929 to 1991.

For the winter months we used regression techniques on the predominantly well-mixed, vertically isothermal profiles with excellent results. For the summer we applied a Feature Model which extracted physically significant depths and gradients from the observations. These modeled data were statistically compared with mixed results indicating little link between SST and mixed-layer depth but good correlation between SST and thermocline gradient.

We believe interannual variability and significant sampling errors in our data contributed to our mixed results. Overall, we feel our approach is robust and has potential for further applications providing data quality issues are addressed.

14. SUBJECT TERMS Feature Model, thermal structure, sea surface temperature, mixed-layer depth, thermocline, gradient, regression.

15. NUMBER OF PAGES 91

16. PRICE CODE

17. SECURITY CLASSIFICATION OF REPORT	18. SECURITY CLASSIFICATION OF THIS PAGE	19. SECURITY CLASSIFICATION OF ABSTRACT	20. LIMITATION OF ABSTRACT
Unclassified	Unclassified	Unclassified	UL

NSN 7540-01-280-5500

Standard Form 298 (Rev. 2-89)
Prescribed by ANSI Std. 239-18 298-102

Approved for public release; distribution is unlimited.

YELLOW SEA THERMAL STRUCTURE

by

Charles R. Fralick, Jr.
Lieutenant, United States Navy
B.S., University of South Carolina, 1989

Submitted in partial fulfillment
of the requirements for the degree of

MASTER OF SCIENCE IN METEOROLOGY AND PHYSICAL OCEANOGRAPHY

from the

NAVAL POSTGRADUATE SCHOOL
September 1994

Author: [redacted]

Charles R. Fralick, Jr.

Approved by: [redacted]

Peter C. Chu, Thesis Advisor

[redacted]

Steven D. Haeger, Co-Advisor

[redacted]

Robert H. Bourke, Chairman
Department of Oceanography

ABSTRACT

There exists a need in the oceanography community to be able to produce climatologies of remote or poorly sampled shallow water areas through remote sensing techniques. Our goal was to construct a three-dimensional thermal structure of the Yellow Sea based primarily upon sea surface temperature data. The ability to do this successfully could lead the way to applying these techniques elsewhere using remotely sensed SST. The shallow water and dynamic conditions of the Yellow Sea made it an ideal study area. The large MOODS observational data set for the area provided us with 15,000 observations from 1929 to 1991.

For the winter months we used regression techniques on the predominantly well-mixed, vertically isothermal profiles with excellent results. For the summer we applied a Feature Model which extracted physically significant depths and gradients from the observations. These modeled data were statistically compared with mixed results indicating little link between SST and mixed-layer depth but good correlation between SST and thermocline gradient. We believe interannual variability and significant sampling errors in our data contributed to our mixed results. Overall, we feel our approach is robust and has potential for further applications providing data quality issues are addressed.

TABLE OF CONTENTS

LIST OF FIGURES

ACKNOWLEDGMENTS

The author would like to acknowledge the financial support of the Naval Oceanographic Office and the time and efforts of Steven Haeger and Dr. Mike Carron. Mr. Haeger wrote the Feature Model we used for this study and provided guidance and an abundance of knowledge.

Many thanks to Dr. Peter Chu for his guidance, patience and good humor. He made my work fun and challenging. Laura Ehret and Mike Cooke provided and abundance of programming assistance, suggestions and their help was greatly appreciated. Dr. Everett (Skip) Carter shared his wealth of statistics knowledge with me and always had the right solution the problems I had.

A special thanks to Kay, my wife, for her patience and encouragement.

I. INTRODUCTION

Satellite remote sensing provides global scale surface parameters such as sea surface temperature, wind speed and heat flux for oceanographic studies. Determination of sub-surface ocean structure from surface parameters becomes important for effective utilization of these satellite data. While in-situ data collection will probably never be replaced by remote sensing techniques, the ability to produce three-dimensional climatological data bases may be possible using remote sensing methods. Of specific interest are those areas where we lack good climatological information either due to lack of sampled data or highly variable conditions which render traditional evaluation ineffective. The latter problem applies to shallow water regions which undergo many short term or seasonal vertical structure changes. In many of these areas there is no permanent or semi-permanent deep thermocline to lend some consistency to shallow profiles. Without some portion of the vertical structure remaining fairly constant there must be a flexible and robust method to attempt to link surface and sub-surface features. The method must be physically sound and applicable over areas large enough to be useful to the oceanographer and tactically significant to naval forces. The Yellow Sea stands out as a prime location to attempt to develop such a method. Shallow water, strong seasonal climate changes and strong forcing both by ocean currents (Kuroshio to the south) and winds set up by monsoons and episodic events make this a highly dynamic area. Additionally,

the area is of great importance both as a major commercial shipping route and as a potential military "hot spot".

A few studies have been completed discussing the relationship of surface conditions to sub-surface structure. Liu *et al.* (1992) have published a study dealing primarily with water mass distribution but it provides no forecasting insight with the exception of generalized locations and characteristics. Haeger (1992) has had limited success developing techniques to determine vertical thermal structure in the Barents Sea from surface temperature but water depth and forcing conditions are significantly different from those in the Yellow Sea. Zhao (1989) discusses in some detail the mechanisms of thermocline formation in the Yellow Sea and their distribution but again does not attempt to develop a predictive link to sea surface temperature. A numerical model was used by Jin *et al.* (1993) to predict vertical thermal structure. Their modeled profiles vaguely followed the shape of the actual profiles but were overly smoothed and indistinguishable. Wan *et al.* (1990) used a similar approach with a one-dimensional, three layer model and produced good results in the shallowest areas of the Yellow Sea but were poor in deeper areas. We will use techniques similar to Haeger (1992) to study the Yellow Sea thermal structure. Our data is a subset of the worldwide Master Oceanographic Observation Data Set (MOODS) and consists of over 50,000 profiles before quality control and binning for desired area coverage. The data cover the years 1929 through 1991 and come from numerous instrument types including XBT's, CTD's, and Nansen bottles.

The basic approach in this study consists of two models for two typical profile "types". Winter profiles for the Yellow Sea

typically display an isothermal structure. A regression analysis will be applied to the winter profiles and the results statistically evaluated. Summer profiles show the familiar three-layer structure of a mixed-layer, thermocline and deep layer. Regression techniques will not be appropriate in this case. In order to provide a basis for comparison of profiles from different locations "characteristics" from each of the summer profiles will be produced. These characteristics must provide a physical interpretation of the profile rather than just temperature-at-depth values. More significant than temperature/depth pairs are gradients of temperature within a layer, mixed layer depth and the depths at which inflection points of the profile occur. To produce these values we must first obtain a high resolution profile of the original observation. This will be accomplished by interpolation from surface to bottom at close interval and will allow determination of inflection points in the profile. Gradient information will be provided by taking the first derivative of the high resolution profile (yielding the slope or gradient). Portions of the profile which are non-linear over two or more interpolation intervals will be modeled using parabola-shaped segments inserted into the "gradient space" profile. These segments will model transition from the mixed-layer to the thermocline and from the thermocline to the deep layer. From this procedure we will then obtain a "characteristic" file containing sea surface temperature, mixed-layer depth, mixed layer gradient, depths for top and bottom of the thermocline, thermocline gradient, depths for top and bottom of the deep layer and deep layer gradient.

Using these methods it is hoped that a physically based, consistent approach can be used over the Yellow Sea in order to construct a three dimensional thermal structure for both the winter and summer seasons.

II. YELLOW SEA METEOROLOGY AND OCEANOGRAPHY

A. METEOROLOGY

As discussed by Nestor (1977), the Yellow Sea area is within the circulation patterns set up by the Asian monsoon. This monsoon pattern generates very cold northwest wind in winter as a result of the Siberian high. The average daily high temperature during January on the Korean Peninsula is near 0°C. During the winter the Jet Stream is positioned just to the south of the Yellow Sea and the Polar Front just north of the Philippines. In addition to the monsoon-derived wind flow, periodic "Shanghai Lows" form over the Yellow Sea providing another source of surface wind stress. Typical February locations for these features are shown in Figure 2.1 and are discussed in detail by Krishnamurti and Surgi (1987) and Boyle (1987). According to the U.S. Navy Regional Climatic Study of the Central East Asian Coast and Associated Waters (Elms, 1989), the mean scalar wind speed in the Yellow Sea reaches a maximum in February with an average of 35 m/sec near the central portion. Mean scalar surface winds over the whole region average nearly 28 m/sec from the north. The change of season begins in March when temperatures are 5°C warmer than in February. Rapid weakening of the Siberian high progresses into April.

In late April the Polar Front has moved northward toward Korea with warm, moist air following behind. Numerous frontally-derived events occur making late April and May highly variable in terms of winds and cloud free days. By May daily high temperatures rise to between 15 and 16°C. During this time period storms originating over

Mongolia may cause strong, warm westerlies carrying yellow desert sand (termed "Yellow Winds").

By late May and early June the summer low pressure system begins to form over Asia. Initially this low pressure area is centered north of the Yellow Sea producing westerly flow. In late June this low begins to migrate to the west setting up the southwest monsoon that dominates the summer months. The winds remain variable through June until strengthening of the Manchurian low occurs. The mean location of the Polar Front is now just south of the Japanese islands of Kyushu and Shikoku. Jet stream position is just south of Korea. Figure 2.1 shows the mean June locations of these features. June also marks, historically, a jump in precipitation associated with the warm, moist air south of the Polar Front (Watts, 1969). Occasionally Okhotsk highs block the northerly progression of the Polar Front. By July, however, high pressure (Bonin high) to the south and the low over Manchuria produce southerly flow carrying warm, moist air over the Yellow Sea.

In August the Polar Front has moved north to a position over North Korea. This is a time of very high temperatures (the mean daily temperature in August is in the 32-35°C range) and very unstable weather conditions. Despite the very active meteorological conditions, June through September have relatively low mean wind speeds of between 18 and 24 m/sec over the central Yellow Sea. By September the mean temperature drops to near 27°C and the Polar Front begins a rapid southerly migration as winter conditions begin to return. October brings the first cold outbreaks and November the onset of winter conditions. Winds in October are variable but begin to show a northerly bias. November mean wind speeds are not as high

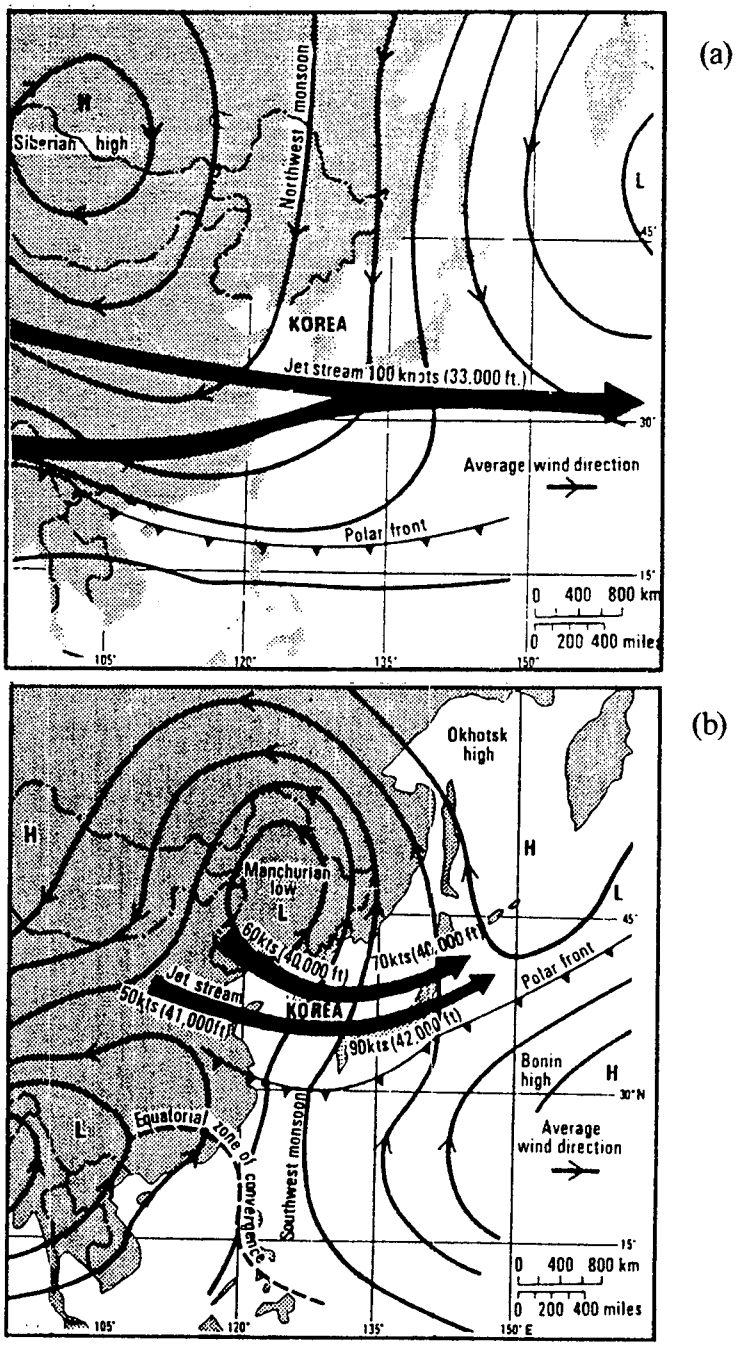

Figure 2.1. Mean locations of pressure systems and winds for the months of (a) February and (b) June. (from Langhill, 1976).

as late winter (around 24-26 m/sec) but the direction is primarily northerly throughout the winter. This completes the annual cycle. Table 2.1 summarizes the annual cycle.

As relevant to oceanographic forcing, the Yellow Sea experiences the strongest surface wind stress in February and March and a minimum of solar insolation during that period. The mean wind stress is lowest and solar insolation is highest in August and September.

B. OCEANOGRAPHY

The Yellow Sea is a semi-enclosed basin covering roughly 295,000 square kilometers and is one of the most developed continental shelf areas in the world (Yanagi and Takahashi, 1993). For purposes of this paper the "Yellow Sea" is defined as the Bohai Sea, Huanghai (Yellow) Sea and northeast portion of the East China Sea. Continental boundaries for this area are mainland China to the north and west and North and South Korea to the east. The 32 degree north latitude line is the southern boundary based upon observational analysis discussed in Chapter III.

While the Yellow Sea covers a relatively large area (roughly 300,000 square kilometers), it is uniformly shallow reaching a maximum depth of about 140 m. The water depth over most of the area is less than 50 m. The deepest water is confined to a north-south oriented trench which runs from the northern boundary south to the 100 m isobath where it fans out onto the continental break. The gradients in slope across the bottom are very small and there are no distinct topographic features seaward of the coastline. Coastline surrounding the Yellow Sea is convoluted, possessing numerous inlets and small islands (Figure 2.2).

<table>
<tr><td>MAR.</td><td>APR.</td><td>MAY</td><td>JUNE</td><td>JULY</td><td>AUG.</td><td>SEP.</td><td>OCT.</td><td>NOV.</td><td>DEC.</td><td>JAN.</td><td>FEB.</td></tr>
<tr><td colspan="3">SPRING</td><td colspan="3">SUMMER</td><td colspan="3">AUTUMN</td><td colspan="3">WINTER</td></tr>
<tr><td colspan="2">North-west Monsoon</td><td colspan="2">Transition period</td><td colspan="3">South-west Monsoon[7]</td><td>Transition period</td><td colspan="3">North-west Monsoon</td></tr>
<tr><td colspan="2">Yellow wind[2]
Foehn[1]</td><td>Late frost[3]</td><td colspan="2">Rainy season
Polar front South of R.O.K.</td><td>Bonin High predominates
Heavy Rain[8]</td><td>24 hour precip exceeds 12 inches owing to typhoon</td><td colspan="2">Under influence of migratory high, elongated east-west mean track along 38° N.[10]</td><td colspan="2">Heavy snow may be expected along Taebaek Mts with strong north to south pressure gradient (high to north)</td></tr>
<tr><td colspan="3">Blocking due to slow-moving Mongolian high results in cut-off low over Yellow Sea.</td><td>Pressure higher to east.</td><td colspan="3">High pressure area to south; low to north.</td><td colspan="3">High pressure area to west; low to east</td></tr>
<tr><td colspan="4">Korea under influence of migratory high [4]</td><td colspan="3">Typhoons may affect R.O.K.[9]</td><td colspan="3">Exceptionally good visibility over long distance within migratory high area.[11]</td><td colspan="2">3 cold and 4 warm day cycle prevails over Korea.</td></tr>
<tr><td colspan="2">Gust winds[5]
Taiwan lows</td><td colspan="2">Frontal thunderstorms duration 1–2 hrs. up to twice per month.[6]</td><td colspan="3">Airmass thunderstorms, 5–10 km. diameter; 2–5 per month.</td><td>Frontal thunder-storms, 0–2/month</td><td colspan="2">Shanghai low may develop and affect R.O.K.</td><td>Taiwan lows frequently affect R.O.K.</td></tr>
<tr><td colspan="2">Sea fog, most frequent in July over Inchon area. Frontal and radiation fog may occur occasionally.</td><td colspan="4">Radiation and frontal fogs occur frequently, however duration is short. Radiation fog seen inland.</td><td colspan="4">Siberian airmass dominates Korea.</td></tr>
</table>

[1] North China low passing over North Korea causes foehn (hot, dry south to easterly flow) over west and central sectors of R.O.K.
[2] Mongolian low passing over southern Manchuria causes yellow winds (strong, dry west wind carrying yellow dust).
[3] Late frost may occur when migratory high predominates over R.O.K.
[4] Mean track of migratory high is along 33° N.
[5] Low over Shantung Peninsula may cause gusty winds over R.O.K.
[6] Intense frontal thunderstorms in May signal approach of rainy season.
[7] Cool summer and drought if South-west Monsoon weak and Okhotsk High intense.
[8] Heavy rain-latter part of rainy season.
[9] Hot and humid with maritime tropical air intrusion. None or as many as two tropical storms or typhoons from end of June through September may affect R.O.K.; least likely in August owing to Bonin High.
[10] Migratory highs move at about 20 knots, speed up with northward movement and vice versa.
[11] Often precedes bad weather.

Table 2.1. Climatic calendar for South Korea and surrounding seas. (Langhill, 1976).

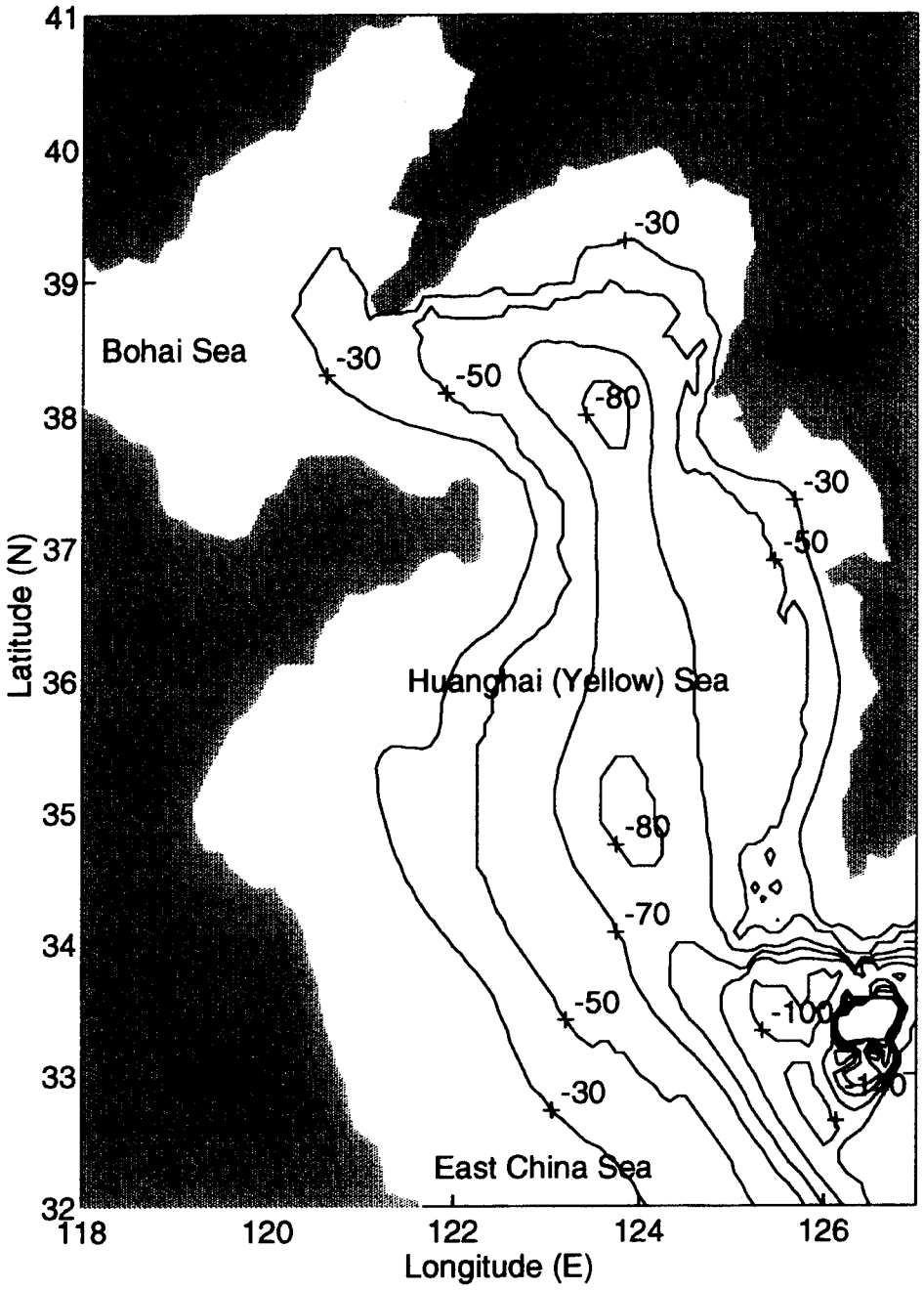

Figure 2.2. The Yellow Sea study area with isobath contours. Bathymetry information is from the NGDC and Naval Oceanographic Office DBDB5 world bathymetry data bases. Depths are in meters (m).

The circulation in the Yellow Sea is primarily forced by monsoonal winds and strong surface heat fluxes (Yanagi and Takahashi,1993). Water mass formation is a result of the interaction of forces as well as river runoff and the intrusion of East China Sea and Kuroshio Water from the south. Li and Yuan (1992) used a theoretical approach to analyze the circulation and water mass formation mechanisms and their results agreed quite well with observed data. One significant feature is the cold bottom water mass in the central Yellow Sea called "Cold Water Mass in the Yellow Sea" (CWYS) by Li and Yuan. The CWYS is not a result of intrusion by Kuroshio or East China Sea Water but is locally generated. During summer CWYS has been observed and modeled to circulate cyclonically with corresponding vertical upwelling in the center and downwelling at the edges. According to Li and Yuan the vertical convection occurs within a thin layer near the thermocline and does not persist all the way to the bottom. Su and Weng (1994) use the principle of modified water masses to construct a picture of the circulations and water masses of the Yellow Sea (Figure 2.3). Yanagi and Takahashi (1993) describe a similar circulation pattern but also say that the summer circulation reverses itself near the bottom. Their study shows that the Yellow Sea circulates anti-cyclonically from surface to bottom during winter. Figure 2.4 shows the regional circulation patterns for the Yellow Sea and surrounding areas (Guan, 1994).

An analysis by Liu *et al.* (1992) describes a complex water mass structure in the Yellow Sea based upon temperature and salinity properties. Generally the area can be divided into the central Yellow Sea, coastal areas, the area subject to intrusion (southern

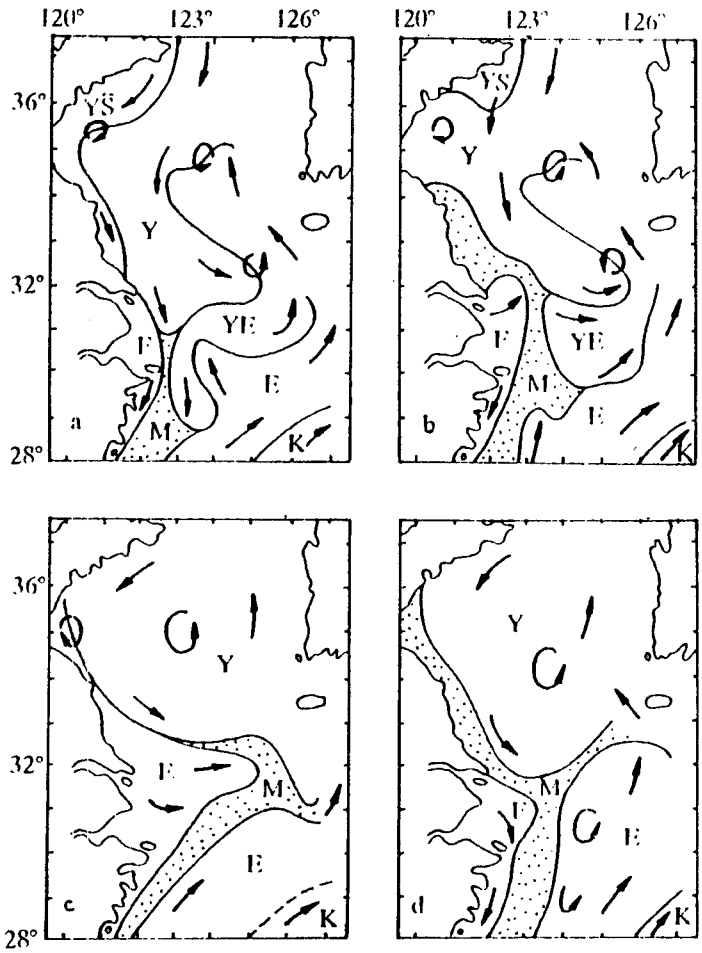

Figure 2.3. Modified water mass distribution and circulation patterns in the Yellow Sea for; a) February; b) May; c) August; d) November. Y - Yellow Sea mixed water, YS - Yellow Sea nearshore water, YE - Yellow Sea and East China Sea mixed water, E - East China Sea mixed water, M - fully mixed water, K - Kuroshio water, F - Continental coastal diluted water (from Su and Weng, 1994).

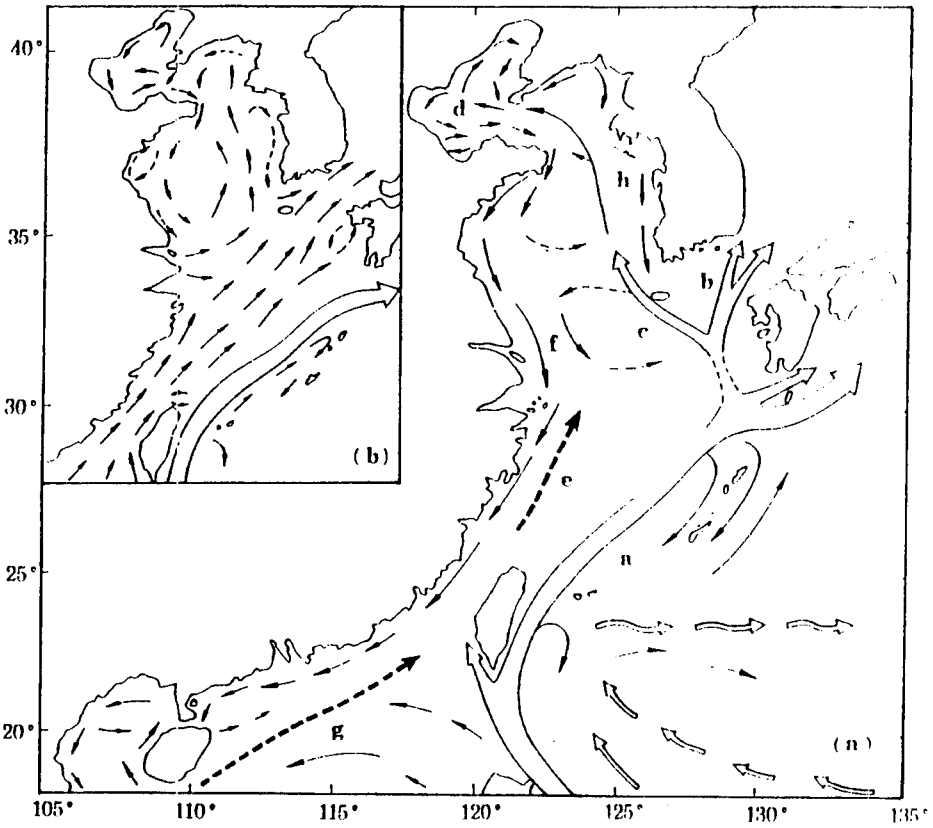

Figure 2.4. Regional circulation patterns for the Yellow, Bohai and East China Seas for winter(a) and summer (b). a, Kuroshio; b, Tsushima Warm Current; c, Yellow Sea Warm Current; d, Bohai Sea Circulation; e, Taiwan Warm Current; f, China Coastal Current; g, South China Sea Warm Current; h, West Korea Coastal Current (from Su and Weng, 1994).

Yellow Sea) and the Bohai Sea. Su and Weng (1994) make a similar analysis. When considering temperature characteristics alone, the central region stands out due to its cold bottom water. As summer brings strong surface heating, this cold water produces the sharpest thermocline gradients in the region. During winter this water provides a significant buffer preventing central water temperatures from reaching the near-freezing temperatures that the nearshore regions experience. The nearshore regions generally follow air temperature trends with the coldest sea surface temperatures being found to the north in the Bohai Sea during winter and warmest on the east and west boundaries during summer. The Bohai Sea maximum surface temperature is moderated in summer due to significant river discharge by the Huang River. In the very nearshore, large tidal ranges (more than 10 m at Inchon) cause strong mixing and near homogeneous thermal structure year round.

III. MIXED-LAYER DYNAMICS

A. THEORY

The observed vertical temperature profiles in the Yellow Sea exhibit two dominant shapes, one associated with the winter season and the other with the summer season. Both of these profile types are represented in Figure 3.1 by plots of two observations from the Yellow Sea. There are transitional profiles with different degrees of stratification but all follow the basic shape of one of the two types. Based upon the presence of a vertically uniform surface layer (i.e., the ocean mixed-layer) in a majority of the profiles, mixed-layer dynamics is expected to provide a basis for understanding the factors influencing the seasonal profile characteristics.

A simple mixed layer model provides the necessary framework to predict the sea surface temperature by the divergence of vertical heat fluxes

$$\frac{\partial T_s}{\partial t} + u \bullet \nabla T_s = \frac{Q_o - \Lambda(\Pi)\, Q_{-h}}{\rho_o c_p h} \qquad (1)$$

where T_s is the sea surface temperature, u is the horizontal velocity, Q_o is the net surface heat flux (positive sign indicates downward flux), Q_{-h} is the entrainment heat flux, ρ_o is the seawater density, c_p is the specific heat capacity of the seawater (under constant pressure), h is the mixed-layer depth and $\Lambda(\Pi)$ is the Heaviside step function of Π

$$\Pi \equiv C_1 u^3_* - \frac{C_2 \alpha g h Q_o}{\rho_o C_p} \qquad (2)$$

which denotes the surface forcing condition. C_1 and C_2 are tuning coefficients and α is the thermal expansion coefficient. Λ is 1 for strong surface wind forcing where $\Pi > 0$, otherwise Λ is 0.

Turner and Kraus (1967) discuss the relationship between surface forcing (wind stress, surface heat fluxes) and the mixed layer entrainment process. Chu and Garwood, (1991) and Chu et al. (1990) utilize a simple model to parameterize a prognostic equation for mixed-layer depth, h,

$$\frac{\partial h}{\partial t} = w_e - w_{-h}. \qquad (3)$$

with w_e representing the vertical velocity at the base of the mixed-layer and w_{-h} representing the rate of change of the mixed-layer depth. Considering the turbulent kinetic energy and only considering work by the surface wind and bouyant damping (forcing) due to surface heating (cooling) as sources and sinks we can parameterize entrainment velocity with

$$w_e = \frac{\Pi}{gh\alpha\,(T_s - T_{-h})} \qquad (4)$$

where w_e is the vertical velocity at the mixed-layer base produced by interior oceanic dynamics or Ekman pumping. Finally, we arrive at two heat equations with one for the entrainment regime and the other for the shoaling regime.

$$\frac{\partial T_s}{\partial t} + u \bullet \nabla T_s = -\frac{Q_{-h} - Q_o}{\rho_o c_p h} \tag{5}$$

$$\frac{\partial T_s}{\partial t} = u \bullet \nabla T_s = \frac{Q_0}{\rho_0 c_p h} \tag{6}$$

B. APPLICATION TO THE YELLOW SEA

With both the mean annual maximum surface wind speed and solar insolation minima occurring in February, conditions favor an entrainment regime. Evaluation of the data supports this since there is an almost complete lack of significant stratification during the winter months. With strong winds and low positive or negative surface heat flux, entrainment dominates dynamically. Hence, it follows that temperature profiles should be nearly isothermal. Deviations from this do occur which may, in part, be explained by episodic meteorological events and local mesoscale influences such as river runoff or ice formation.

During the summer months surface wind speeds are at a relative minimum and solar insolation at maximum values (with August being the minimum wind speed month). This strong positive heat flux into the ocean combined with lower wind stress favors a shoaling regime. As evidenced by the collected data, this mixed-layer/thermocline structure makes up the majority of the profiles. As discussed previously, the summer season is subject to numerous tropical disturbances, storms and typhoons. These episodic events may cause periodic bursts of high surface wind stress and subsequently deeper mixed-layers or in rare cases isothermal conditions.

These regimes hold true through the previously defined seasons. During the transition periods of May and November a mixture of both regimes may occur. It would appear that a combination of analytical methods would be required for these months.

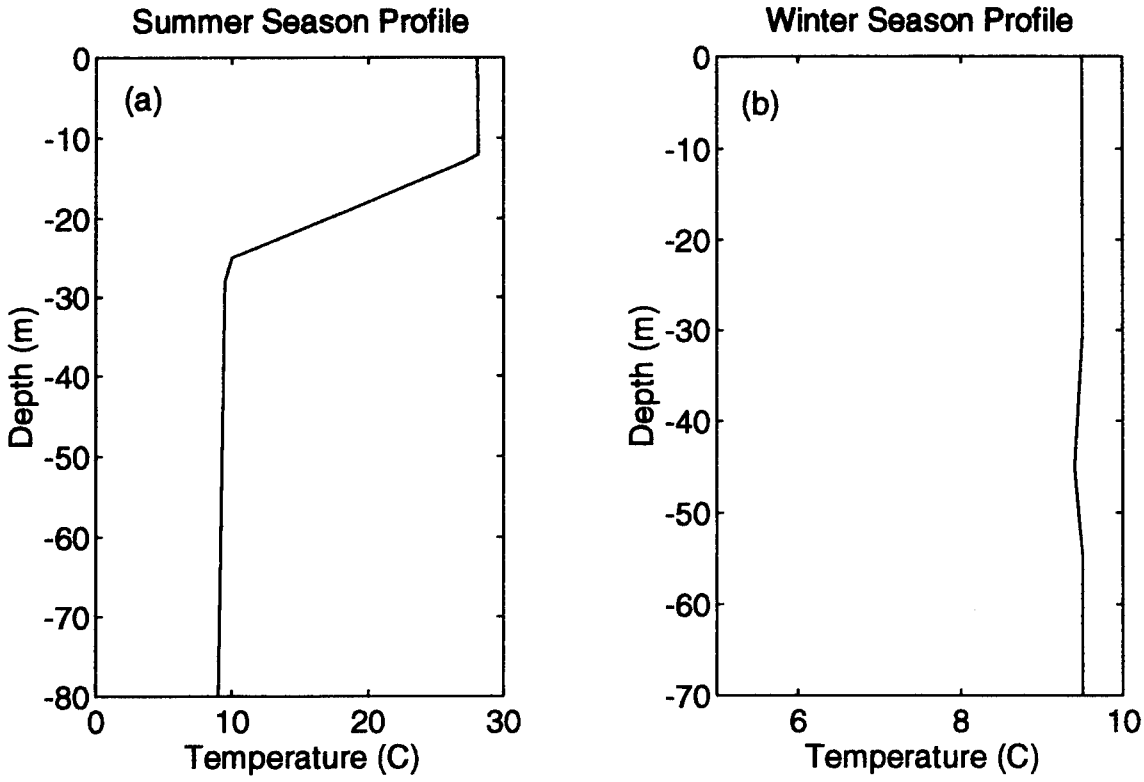

Figure 3.1. Typical seasonal profiles for; (a) Summer (August) 1972, in the central Yellow Sea and (b) Winter (February) 1969 in the central Yellow Sea. Both observations are from the MOODS observational data base.

IV. METHODS

A. INITIAL DATA ANALYSIS AND BINNING

The MOODS data set is a compilation of all reported observations over all the world's oceans. Due to the shear size (several million profiles) and enormous influx of data, quality control is a difficult task. Erroneously recorded locations or poorly recorded profile data are archived as reported. The study domain covers the area 32°-41°N and 118°-127°E and the data set within this area initially consisted of just over 15,000 profiles covering a time span from 1929 to 1991.

The first disqualification criteria for profiles was based upon bathymetry. As there are no areas within the established boundaries that are deeper than 150 m, a binning program was constructed which discarded any profiles that extended to depths greater than 150 m. This initial quality control discarded 50 profiles. As a next step in quality control, unusual or "oddball" profiles were inspected for possibly erroneously recorded data. If profiles were drastically different than other profiles in the area and time frame, they were discarded as a conservative approach. This quality control step discarded another 15 profiles. The final data set consisted of 14,989 profiles.

To aid in visualizing the vertical thermal variability of profiles during the winter months, a series of scatter plots was generated of sea surface temperature (SST) versus the temperature at 30, 50, 70 and 100 m. These plots allow qualitative evaluation and give the analyst a chance to see early trends in the data and

determine what later analysis may be useful. Additionally, for the summer months, mixed layer depth (MLD), thermocline gradient and thermocline differential temperature data were gridded over the area and contoured. In order to make this data more useful during analysis they were continuously interpolated between contours to produce color shaded images. SST for all months was done in a similar manner. These plots are shown and discussed in Chapter V.

B. WINTER SEASON ANALYSIS

Our initial evaluation resulted in designating December, January, February, March and April as the winter season. Climatology of the Yellow Sea and studies previously mentioned revealed that the winter season thermal structure is very uniform in the vertical due to buoyant instability and strong wind forcing. A regression analysis of SST versus temperature at depth was performed on the winter months at 30, 50, 70 and 100 m and the correlation coefficients, CC(i,j), for the temperature values at the different levels were calculated for the profiles

$$CC(i,j) = \frac{\sum (T_i - \overline{T_i}) \bullet (T_j - \overline{T_j})}{\sqrt{\sum (T_i - \overline{T_i})^2} \bullet \sqrt{\sum (T_j - \overline{T_j})^2}} . \qquad (7)$$

T_i denotes the observed temperature at the ith level, T_j denotes the observed temperature at the jth level and overbars represent the mean values of the ith and jth level components. Additionally, the standard deviation of the winter data set is calculated and plots of sea surface temperature versus temperature at depth and the regression line were produced.

C. SUMMER SEASON ANALYSIS

Summer is comprised of June, July, August, September and October in our study. Most summer profiles exhibit the mixed layer, thermocline and deep layer profile characteristics. To grasp the major features of the profiles, a feature model has been developed in the Naval Oceanographic Office (Haeger, 1992) for diagnosing ocean thermal structure from observational temperature profiles. The model was originally called the Gradient Model. Several parameters, which represent major characteristics of each temperature profile, are SST, MLD, thermocline depth and thermocline temperature difference. The feature model transforms each profile into a set of these parameters. The feature model contains three components or steps: (a) a "first guess" feature model, (b) high-resolution profiles interpolated from observations, (c) fitting of the high resolution profiles to the feature model.

1. Gradient space

If we consider profiles in gradient space, i.e., $G_T = \partial T(z)/\partial z$, each profile can be represented by the SST plus gradients below the surface, e.g.,

$$[SST, G_T(0, z_1), G_T(z_1, z_2), \ldots, G_T(z_{n-1}, z_n)] \qquad (8)$$

for the temperature profile. Here, $n + 1$ is the number of data points and z_i ($i = 1,2,\ldots,n$) are the depths of the data points. For example, 100 temperature/depth points would produce 99 gradient values. If SST is included, we have the same amount of data in gradient space as we had in the original temperature space data. Gleaning physical meaning from a large number of gradient/ inflection point combinations is difficult.

2. Feature model

Observation shows that the summertime Yellow Sea exhibits a layered structure (Figure 3.1). Based on the continuity of T and $\partial T/\partial z$ at the interface of any two layers, a feature model (or model to extract physically significant features) can be constructed as:

$$\hat{T}^{(m)}(z) = G_T^{(m)} z + SST, \quad z \in [-d_1, 0]$$

$$\hat{T}^{(en)}(z) = \frac{(z+d_1)}{(d_2-d_1)} \left[(G_T^{(m)} - \overline{G}_T^{(en)}) z + d_2 G_T^{(m)} - d_1 \overline{G}_T^{(en)} \right] + \hat{T}^{(m)}(-d_1), \quad z \in [-d_2, -d_1]$$

$$\hat{T}^{(th)}(z) = G_T^{(th)}(z+d_2) + \hat{T}^{(en)}(-d_2), \quad z \in [-d_3, -d_2]$$

$$\hat{T}^{(tr)}(z) = \frac{(z+d_3)}{(d_4-d_3)} \left[(G_T^{(th)} - \overline{G}_T^{(tr)}) z + d_4 G_T^{(th)} - d_3 \overline{G}_T^{(tr)} \right] + \hat{T}^{(th)}(-d_3), \quad z \in [-d_4, -d_3] \tag{9}$$

$$\hat{T}_1^{(d)} = G_T^{(d1)}(z+d_4) + \hat{T}^{(tr)}(-d_4), \quad z \in [-d5, -d4]$$

$$\hat{T}_2^{(d)}(z) = \frac{(z+d_5)}{(H-d_5)} \left[(G_T^{(d1)} - \overline{G}_T^{(d2)}) z + H G_T^{(d1)} - d_5 \overline{G}_T^{(d2)} \right] + \hat{T}_1^{(d)}(-d_5), \quad z \in [-H, -d_5]$$

where $(\hat{T}^{(m)}, \hat{T}^{(en)}, \hat{T}^{(th)}, \hat{T}^{(tr)}, \hat{T}_1^{(d)}, \hat{T}_2^{(d)})$ are modeled temperatures of the mixed-layer, entrainment zone, thermocline, transition zone and the first and second deep layers. H represents the water depth, d_1 the mixed layer depth, d_2 the depth at the top of the thermocline, d_3 the depth at the base of the thermocline, d_4 the depth at the top of the first deep layer and d_5 is the base of the first deep layer. Figure 4.1 shows the temperature and gradient space representations of these features. At this point we assume

constant vertical temperature gradients in the mixed-layer ($G_T^{(m)} \approx 0$) in the thermocline ($G_T^{(th)}$) and in the first deep layer ($G_T^{(d1)}$). We assume the gradients are linearly varying with z in the entrainment zone, transition zone and the second deep layer with average values ($\overline{G}_T^{(en)}, \overline{G}_T^{(tr)}, \overline{G}_T^{(d2)}$). By forcing the feature model (9) to each observed profile shape, we should have a "first guess" of the five depths (d_1, d_2, d_3, d_4, d_5) and a high resolution of temperature/depth points in the vertical to obtain the six vertical temperature gradients ($G_T^{(m)}, G_T^{(th)}, G_T^{(d1)}, \overline{G}_T^{(en)}, \overline{G}_T^{(tr)}, \overline{G}_T^{(d2)}$). This treatment extracts the most important features from the observational data and allows direct comparison of profiles via their feature composition.

3. High Resolution Profiles (HP) interpolated from observations

Each of the MOODS profiles is linearly interpolated in the vertical to high resolution (Δz = 0.5 m). As an example, we can denote temperature $Tj = T(z_j)$ where $z_j = z_{j-1}$ - 0.5 m ($z_o = 0$). Each observed profile is tagged with NAVOCEANO's DBDB5 bathymetry data base to provide the water depth H. When the five depths (d_1, d_2, d_3, d_4, d_5) are known, we can divide the data set $HP = (z_j, T_j)$ into six sections: 1) mixed-layer, 2) entrainment zone, 3) thermocline, 4) transition zone, 5) the first deep layer and 6) the second deep layer. For each section or layer we fit (T_j, z_j) to the feature model (9) and obtain the six vertical temperature gradients ($G_T^{(m)}, G_T^{(th)}, G_T^{(d1)}, \overline{G}_T^{(en)}, \overline{G}_T^{(tr)}, \overline{G}_T^{(d2)}$).

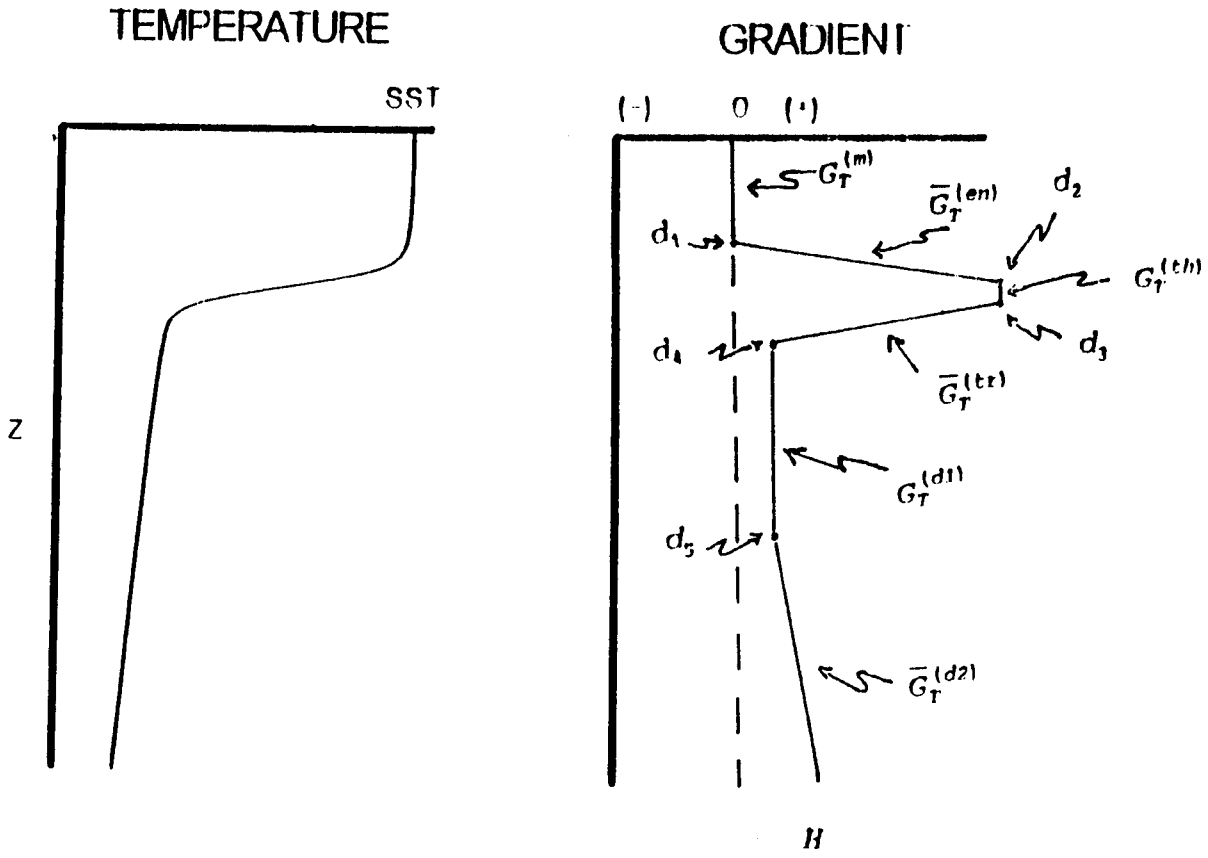

Figure 4.1. The temperature and gradient space representations of the features or profile characteristics modeled by the Feature Model. See the text for a complete discussion of the terms.

4. Iteration method to obtain the Modeled Profile (MP)

A modeled profile (*MP*) with a 0.5 m resolution can be obtained by using the feature model (9) if the five depths (d_1, d_2, d_3, d_4, d_5) are given. Prior to processing the data the depths are not known and vary substantially from profile to profile. To obtain the optimal *MP* we use the iteration method.

We begin with a set of "first guess" values of the 5 depths and 3 gradients,

$$D^0 = (d_1^{(0)}, d_2^{(0)}, d_3^{(0)}, d_4^{(0)}, d_5^{(0)}),$$
$$G_T^{(0)} = (G_T^{(m_0)}, G_T^{(th_0)}, G_T^{(dl_0)}). \tag{10}$$

In this study the "first guess" values are

$$D^{(0)} = (20m, 24m, 32m, 38m, H)$$
$$G_T^{(0)} = (0, -0.5^\circ C/m, -0.005^\circ C/m).$$

We fit the feature model (9) to each profile *HP*, since we know the depths and gradients, and obtain a 0-th order modeled profile, called $MP^{(0)} = (z_i, \hat{T}_j^{(0)})$. The root mean square error (RMS) for the mismatch of *HP* to $MP^{(0)}$ is computed by

$$RMS^{(k)} = \sqrt{\frac{1}{n}\sum_{j=1}^{n} (\hat{T}_j^{(k)} - T_j)^2} \tag{11}$$

where k=0. $RMS^{(0)}$ is expected to be large.

Next, we apply the iteration technique to obtain the optimal *MP* for each *HP* profile. Each of the depths can be adjusted one vertical grid point for one iteration cycle (Δz or $-\Delta z$). For the kth order (k starting from 0, the "first guess") set of depths, $D^{(k)}$, we have 242 ($=3^5 - 1$) possible combinations of depth adjustment,

$$
\begin{aligned}
D_m^{(k+1)} &= D^k + \delta D_m^{(k)} \\
\delta D_1^{(k)} &= (d_1^{(k)} + \Delta z, d_2^{(k)}, D_3^{(k)}, d_4^{(k)}, d_5^{(k)}) \\
\delta D_2^{(k)} &= (d_1^{(k)} - \Delta z, d_2^{(k)}, D_3^{(k)}, d_4^{(k)}, d_5^{(k)}) \\
&\vdots \\
\delta D_{242}^{(k)} &= (d_1^{(k)}, d_2^{(k)}, D_3^{(k)}, d_4^{(k)}, d_5^{(k)} - \Delta z).
\end{aligned}
\tag{12}
$$

We therefore use (9) to produce 242 modeled profiles, among which we pick up a profile with the minimum RMS error as the $(k + 1)$th order set of depths, $D^{(k+1)}$. This procedure is repeated until the minimum RMS error is achieved. If the number of iterations reaches a prescribed limit (400), the iteration process is stopped and the RMS error is compared to a prescribed criterion (0.5°C). If RMS < 0.5°C, we obtain an optimal set of depths and gradients. If RMS > 0.5°C, we reject the feature model (9), i.e., the *HP* profile cannot be fitted by the feature model. These rejected profiles are discarded.

5. Flat and sloping bottom versions of the Gradient (Feature) Model

There are currently two versions, flat bottom and sloping bottom, of the Gradient Model of which we use the latter. In the original, flat bottom version the program required that a maximum depth be entered to perform calculations to. This depth then became, in effect, the depth of all profiles. This resulted in errors due to sloping bottom biasing where deep profile features could be missed completely or shifted incorrectly to shallower depths. To overcome this problem, Haeger (1994, personal communication) developed the second, sloping bottom type which requires two depth related inputs. The first is the minimum depth to accept a profile. This prevents extremely shallow profiles from contaminating the data output. Very shallow profiles are almost universally homogeneous in

the vertical in the Yellow Sea and would be of little analytical value. We select a depth of 30 m for the profile minimum. The second input is the percent of the water column a profile must extend to be retained. This allows the gradient and depth calculations to be performed over the individual profile length rather than a preset depth. The bottom cannot be chosen (100%) since not all profiles extend to the bottom. We choose 70% as the cutoff since all profile characteristics are usually contained within this percentage of the profile depth.

6. Model output analysis

The resulting modeled output files and their corresponding de-meaned (perturbation) files were evaluated statistically for mean and standard deviation. The correlation coefficient for one feature versus another was calculated (as in the winter analysis section) and significant results plotted. Both contour plots and continuously shaded color plots are utilized to aid in data analysis.

V. RESULTS

A. WINTER

1. Statistics

Sample sizes for the four depths of interest (30, 50, 70 and 100 m) decrease, as expected, with depth. The 30 and 50 m isobaths cover a large portion of the Yellow Sea area and therefore yield the most observations. The areas encompassed by the 30 and 50 m isobaths contributed 4527 and 3510 observations, respectively, with 1996 and 142 observations at the 70 and 100 m isobaths. The small number of observations available at 100 m suggests that the statistics calculated at this depth may not be completely representative of the thermal structure there. The scatter plots and linear regression results for the winter season are shown in Figure 5.1 for the 30, 50, 70 and 100 m depths. The resulting equation is provided on each plot as well as the correlation coefficient obtained for sea surface temperature as the independent variable and temperature-at-depth as the dependent variable. Table 5.1 summarizes significant statistical results.

The regression equations calculated are similar; all slope coefficients are greater than 0.95 and the intercepts are between 0.67 and 0.96°C. The slope and intercept calculated at 100 m are more similar to the 30 m calculations than those at 50 and 70 m. However, the small sample size at 100 m may, as previously mentioned, bias these results. This was evidenced by the intercept error at 100 m which is much larger than at the other depths. A larger sample population would most likely stabilize the statistical

results at this depth. The slope and intercept at 50 and 70 m are very similar to those at 30 m, indicating uniformity in the data from the surface to at least the 70 m isobath. Standard error for both the slopes and intercepts at the 30, 50 and 70 m depths indicates a good fit for those equations. The confidence limits for the individual equations are provided in Table 5.1 and display low standard error for all of the depths analyzed.

Analysis of the variances for each depth are also provided and, as was expected, show the best results at the 30 m depth and progressively greater error as depth increases. The water closest to the maximum agitation (surface wind forcing) will generally exhibit the best mixing and the best statistical correlation to the surface temperature values. The exception is at 100 m, where lack-of-fit and pure error results are surprisingly good. We attribute this to the small sample size and do not put high confidence in these results. As supporting evidence, we provide the 0.95 confidence limits for the slope and intercept values at 100 m which show greater variance from the mean values than do the other depths. Correlation coefficient calculations show uniformly good results with values of 0.9716, 0.9630, 0.9559 and 0.9544 for the 30, 50, 70 and 100 m depth.

2. Strong mixing, one-layer structure

As solar insolation begins to decrease in October and winds begin to increase, the mixed-layer deepens as the surface becomes less thermally stable and the entrainment rate increases. The first significant cold air outbreak occurs in October (the beginning of the winter monsoon setup) bringing air temperatures which are lower than the sea surface temperature below. Overturning then occurs as

the thermal stability breaks down. The winter months exhibit progressively stronger surface wind forcing and lower solar insolation values leading to thoroughly mixed conditions from the surface to the bottom. As colder air flows over the Yellow Sea, extensive heat loss from the surface serves to further enhance entrainment. This process continues until the water column is nearly isothermal by December and persists until May. This chronology seems to be supported by the high correlation coefficients between the surface temperature and temperature at depth. Higher correlations at the surface and decreasing correlations with depth point to more complete mixing near the surface. The absence of pure isothermal structure in our results (slope of 1 and intercept of 0) may result from interannual variability in the data set and sampling equipment calibration errors.

Considering the depth of the Yellow Sea, the entrainment process affects the whole water column and creates the near-homogeneous profile observed in this study. Coastal regions undergo this modification earlier due to shallower water but the central Yellow Sea also becomes nearly isothermal by December. This pattern of decreasing temperature can be tracked by the sea surface temperature data which were provided in Figures 5.2 and 5.3. As air temperature drops, the coastal regions rapidly equilibrate, followed by the central Yellow Sea region. Initially, the water along the coast becomes more dense than the water in the central region. The resulting density-driven circulation causes the colder water to flow down the sloping basin bottom to the central Yellow Sea. Upwelling in the center brings warmer water to the surface and subsequently

accelerates the adjustment of the central region to nearer air temperature (since heat exchange occurs over an effectively shallower layer of warmer water). This circulation occurs from the surface down to the top of the CWYS until the temperature of the middle and upper layers eventually reaches the temperature of the CWYS. This analysis is supported by the studies of Zhao (1989) and Li and Yuan (1992) and is expected in the absence of some other significant forcing mechanism.

Since the sample size at 100 m was so small, we do not feel that the data produced can be used to quantitatively describe the thermal structure at that depth. We do feel that the data does allow a qualitative analysis since it so clearly follows that of the shallower depths. Since this data set covers a relatively small portion of the Yellow Sea, this is not a significant deficit in the analysis. We believe that a more complete data set for this depth would yield the same results as the other depths analyzed.

B. SUMMER

1. Gradient model output

After running the Feature Model for the summer months the output data set (5 depths and six gradients) was gridded and horizontally interpolated. We have displayed the resulting fields in two forms: continuously shaded color plots and contour plots. The data represent the total (mean + perturbation) fields for their respective variables. We have included MLD, thermocline gradient and thermocline differential temperature in Figures 5.4 through 5.9. The transition months of May and November are included for reference but have been heavily filtered by the model. These plots, therefore, are not necessarily representative of the typical May

or November structure but represent typical transition month profiles which fall under the layered structure type. Scatter plots of SST versus MLD and thermocline depth are shown in Figures 5.10 and 5.11. To facilitate perturbation analysis, the SST anomaly data were plotted versus the MLD, thermocline gradient and thermocline differential temperature anomalies. These scatter plots are shown in Figure 5.12.

It should be noted that, due to the interpolation process and data sparsity in both coastal regions and the western Yellow Sea, the plotted results are subject to error. However, no major misrepresentations were discovered.

2. Statistics

After statistical evaluation of the total fields we determined that the data do not indicate any statistical link between the fields but did point out a significant data anomaly. Correlation coefficients are all below 0.2. The horizontal banding seen in the Figure 5.10 plots is not a functional grouping of the data but sampling error caused by operators "keying" on typical depth increments. When high-resolution data is utilized (filtered for at least 8 sampling depths), these patterns disappear.

Evaluation of the anomaly data did provide some statistically significant results. Figure 5.12 shows the scatter plots of the SST anomaly field versus the other anomalies and the corresponding regression equations and correlation coefficients. The sea surface temperature anomaly versus mixed-layer depth anomaly exhibits the least correlated results with a correlation of only 0.47. The 0.95 confidence level limits are the highest indicating the most variation (highest standard error) from the regression calculated.

We do not feel the mixed-layer depth anomaly provides any significant information. Correlation of the sea surface temperature anomaly versus thermocline gradient anomaly is much better with a value of 0.82. The 0.95 confidence values for the slope and intercept are very close to the best fit and indicate a good statistical relationship between the two anomalies. Correlation of the SST anomaly versus the thermocline temperature difference anomaly is about 0.68 but the 0.95 confidence level slope and intercept margins are still quite good. The statistical results for these three comparisons are summarized in Table 5.2.

3. Weak mixing, multi-layered structure

a. Mixed-layer

By late winter the water throughout the Yellow Sea is very nearly isothermal. During the onset of the summer monsoon, an increase in solar insolation and weakening winds begin the stratification process in the Yellow Sea. We do not expect to see the formation of a significant mixed layer until either wind speeds pick up considerably or solar insolation is reduced. This is supported by our data and can be seen from the progression of the SST and MLD plots (Figures 5.2 and 5.4). Sea surface temperature is uniformly cold up through April with notable warming occurring in May which would suggest an increase in thermal stability due to stratification. There is very little impact upon MLD since wind forcing is nearing its minimum for the year. Therefore, entrainment is not sufficient enough to overcome the stratification due to insolation and the surface continues to warm. The plots of MLD (Figure 5.4) show that, indeed, there is no significant deepening until September. The maximum MLD occurs during the

transition month of November when solar insolation has decreased markedly and winds have picked up.

b. Thermocline temperature difference

This sequence should also be supported by the magnitude of the thermocline temperature difference. Figure 5.8 shows that the thermocline temperature difference increases from a minimum in May to a maximum in both magnitude and extent in July and August. While the magnitude continues to be large in September, the extent is reduced due to cooling of the surface waters as winter approaches and an increase in entrainment due to increased wind speeds. Or, as the entrainment process becomes more vigorous, the surface temperature is reduced and the resulting mixed-layer temperature is closer to the temperature at the base of the thermocline. The largest magnitudes are centered over the central Yellow Sea which supports the presence of the CWYS discussed in Chapter II.

c. Thermocline gradient

Analysis of the thermocline gradient data indicates predictable progression of the magnitudes and extent (Figure 5.6). In early summer (June) we expect to see little or no gradient since the Yellow Sea is still well mixed. By June, as surface heating begins to create stratification in the water column, we expect to see some evidence of a gradient being established. Figure 5.6 supports this analysis with negative gradients of up to -1.0° C/m located throughout the central Yellow Sea region. No gradients were expected along the coastal regions but interpolation errors in the plotting process do indicate some gradient features. None were expected since the coastal region is well mixed all year due to wave and tidal action. It is difficult, however, to delineate the areas

where the stratification does begin since data tends to be very sparse in the nearshore areas. A more complete data set would allow nearshore analysis and would preclude the interpolation errors we observed. The thermocline gradient is directly tied to both the temperature difference across the thermocline and the thickness of the thermocline. This is important since observations in some areas exhibit large temperature differences but thick thermoclines yield relatively small gradients. Fortunately, the majority of the observations are distributed over the central region where the variability of temperature difference and thickness is not large. The Bohai Sea area displays the most variability but very few profiles were available in this region. This indicates that the very nearshore or very shallow regions will continue to present a challenge to our analysis methods.

d. Prominence of the thermocline

July is a month of strong surface heating as witnessed by the sharp increase in SST shown in Figure 5.2. As a result, the prominence of the thermocline should be evident, and is supported by our data. With the presence of the CWYS in the central region a negative gradient in thermocline temperature should be apparent and appears in the central region of Figure 5.6. The presence of this centrally manifested gradient is more obvious in August (Figure 5.6) and shows the increasing gradient as summer progresses. September shows a strong gradient oriented north-south in the central region which suggests the deeper, colder trough water serves to maintain the temperature difference even into late summer. As solar insolation decreases in October and wind speeds begin to pick up, entrainment begins to break down the gradient between the

mixed-layer temperature and the deep layer. This is borne out in the October plot (Figure 5.6) where the north-south orientation is still present but the magnitude of the gradient has decreased significantly.

4. Anomaly analysis

a. Low correlation between SST and MLD anomalies

The poor correlation of SST anomaly to mixed-layer depth anomaly was not unexpected due to the factors influencing this relationship. While a positive SST anomaly (higher than normal SST) would seem to indicate a shallower mixed layer depth (or negative mixed-layer depth anomaly), the contemporary surface wind forcing data would also have to be considered. All other factors being equal, a positive SST anomaly would lead to a shallower mixed-layer depth. But if the higher SST was accompanied by an increased surface wind speed due to a passing tropical storm or other episodic event, the mixed-layer depth may increase. Figure 5.12a indicates a broad spread of data points and, based upon the meteorological climatology, we submit that this is typically the case. Though surface wind speeds are relatively weak in the summer, tropical storms, occasional typhoons and the movement of the Polar Front back to the south promote variable wind speeds and surface temperature (particularly late in the summer). A multi-variable analysis would probably be required to adequately resolve any correlation between the SST anomaly and the mixed-layer anomaly.

b. High correlation between SST and thermocline gradient anomalies

With the occurrence of a positive SST anomaly, the temperature at the top of the thermocline is expected to increase somewhat barring large changes in the surface wind forcing.

However, there is always a lag in the response time of the water column to SST changes. The less than one-to-one slope of the regression fit in Figure 5.12b perhaps indicates this delay. Variability (standard error) around the regression fit would seem to indicate surface wind forcing variability (or a surface wind anomaly). If there is significant wind forcing corresponding to a positive SST anomaly, the water column will undergo both a positive heat flux and an increase in entrainment. Since the thickness of the mixed-layer would increase in this scenario, the thickness of the thermocline for a given observation point would decrease. If the resulting mixed-layer temperature remained near the original, pre-perturbation value, a net thermocline gradient increase would be observed. Thus a positive SST anomaly in this case would produce a positive thermocline gradient anomaly. A variety of combinations could be discussed in which the SST anomaly could result in positive or negative thermocline gradient anomalies.

Another factor to consider is the deep layer stability. Because of the nearly constant temperature of the CWYS mass in the central Yellow Sea, it acts as an anchor and is relatively immune to any SST or mixed-layer temperature changes. With an increase in the water temperature above, an increase in the gradient of the thermocline would result. A decrease in the water temperature above would result in a decrease of the thermocline gradient. This appears to be the most important consideration since our data points to a direct relationship between SST anomaly and thermocline gradient anomaly. Figure 5.13 depicts this relationship. Again, the variability of data from the regression fit would indicate variability in surface wind forcing conditions.

c. Correlation between SST and thermocline temperature difference anomalies

More variability is evident in the results of the SST anomaly versus thermocline temperature difference anomaly. While the temperature at the base of the thermocline is held relatively constant, the base of the mixed-layer, of course, is not. As solar insolation increases during cloud-free days or a warm front passes through the region, the SST increases. Given a constant wind speed, the resulting mixed-layer will be warmer and will shoal following the principles of Turner and Kraus (1967). Given enough information, it would be straightforward to calculate this change following a prognostic model such as that formulated by Chu and Garwood (1991). However, with substantial changes in wind speed the resulting change in mixed-layer temperature would depend upon the resulting entrainment rate and could become either warmer or cooler. With the generally weak surface wind stress in the summer we suggest that, despite much variability, the anomalies in thermocline temperature difference typically follow the SST anomalies. There is better correlation here than with the SST anomaly versus MLD anomaly because any change in mixed-layer temperature results in a change in thermocline temperature difference. This relationship does not hold true in all cases for the SST versus MLD anomaly comparison since entrainment rate is forced not only by temperature change, but by wind stress change. A correlation of 0.69 is not overwhelming, however, and the same factors which influenced variability in the SST anomaly versus mixed-layer depth anomaly are present here. The difference in this case is that the temperature at the top of the thermocline is governed by mixed-layer

temperature. The mixed-layer temperature cannot increase without SST increase, thus providing a direct link. We believe that further analysis over a smaller area would show a better correlation of the data. In particular, the central Yellow Sea region with the CWYS below and deeper water should exhibit good correlation since short term fluctuations in temperature are less likely to cause rapid changes in deeper water and cannot overcome the stability of the CWYS water.

C. SUMMARY OF RESULTS

The winter season analysis was very straightforward and produced very good statistical results. However, there were some deviations from the "ideal results" which should be noted. For the strong mixing, one-layer conditions which exist throughout the winter months, we expected very nearly isothermal profiles to prevail. The statistics show slight variation from a one-to-one slope and an even spread of data for the 0.95 confidence intervals. These results suggest that combining all winter months into the "winter season" has introduced interannual variability into what might be much better results. From one year to the next there may be subtle variations in the rate of overturning, solar insolation and wind forcing. Teleconnection from episodic, distant forcing mechanisms and years of high precipitation and storm frequency may all lend lack of coherency to this composite grouping of data. If the data were sufficient in size, spatial regularity and temporal resolution, a time series analysis of individual months and years would, we believe, show true isothermal structure. We binned one particularly well-sampled year (1969) for the months of January, February and March in a fairly small area (1 degree

square) in the central Yellow Sea. When the data were analyzed using the same winter season methods previously applied, the results were indeed better. The correlation for each month was 0.97 or better and slopes were 0.975 or better. When this same area was binned to exclude all but high resolution profiles (at least 8 sample points in the profile), the results were better still. While the relatively small number of profiles in the area could lend some lack of credibility to these results, we believe the tendency of the results is important. Clearly the higher resolution data produces statistical results which depict the thermal structure which should exist based upon physical principles. Quality data is very important to the successful implementation of our modeling techniques and any other analytic approach.

The summer results were a combination of good and bad results. While there are obviously many possible combinations of wind stress and surface heating magnitudes during the summer, we expected better correlation of SST anomaly to mixed-layer depth anomaly. Failure to achieve these results may stem from several factors. One which we believe is key is, again, poor data quality. The banding patterns in the scatter plots of SST versus mixed-layer depth are caused by operator errors in data collection and analysis. The fact that these patterns disappear when using only CTD data are used indicates serious flaws in the interpretation of XBT data. Many observations were taken prior to CTD and even XBT technology. While their results may be no less accurate, they are certainly less highly resolved in the vertical. Perhaps with the higher resolution of CTD data we would have observed some relationship of SST anomaly to mixed-layer depth anomaly. To test this hypothesis we again

binned a relatively well sampled area (central Yellow Sea, September, 1972) for high resolution profiles (8 or more points), ran the Feature Model and analyzed the model output. Correlation of SST anomaly to mixed-layer depth anomaly increased from below 0.5 in our previous results to 0.74. We must emphasize that the small sample size was not statistically robust but the tendency for all comparisons to improve is significant. Today, NOAA vessels utilize an automated XBT recording and analysis system which may eliminate some of the sampling errors observed in our XBT data. We submit that this may be a worthwhile consideration for military vessels in the future.

The ability of the Feature Model to extract physical feature characteristics from observations is very good. In tests of the model against standards we consistently observed very good agreement between the model and actual data. The model does have a tendency to indicate shallower mixed-layer depths than actually exist but the errors were minor in most observed instances. The RMS error calculation and iteration process removed 5 percent of the profiles from the summer data set. Considering that most of the removed profiles were in very shallow (less than 30 m) water, we feel these results are acceptable. Review of rejected profiles consistently shows good "skill" by the model and gives us confidence in its ability to detect major profile features.

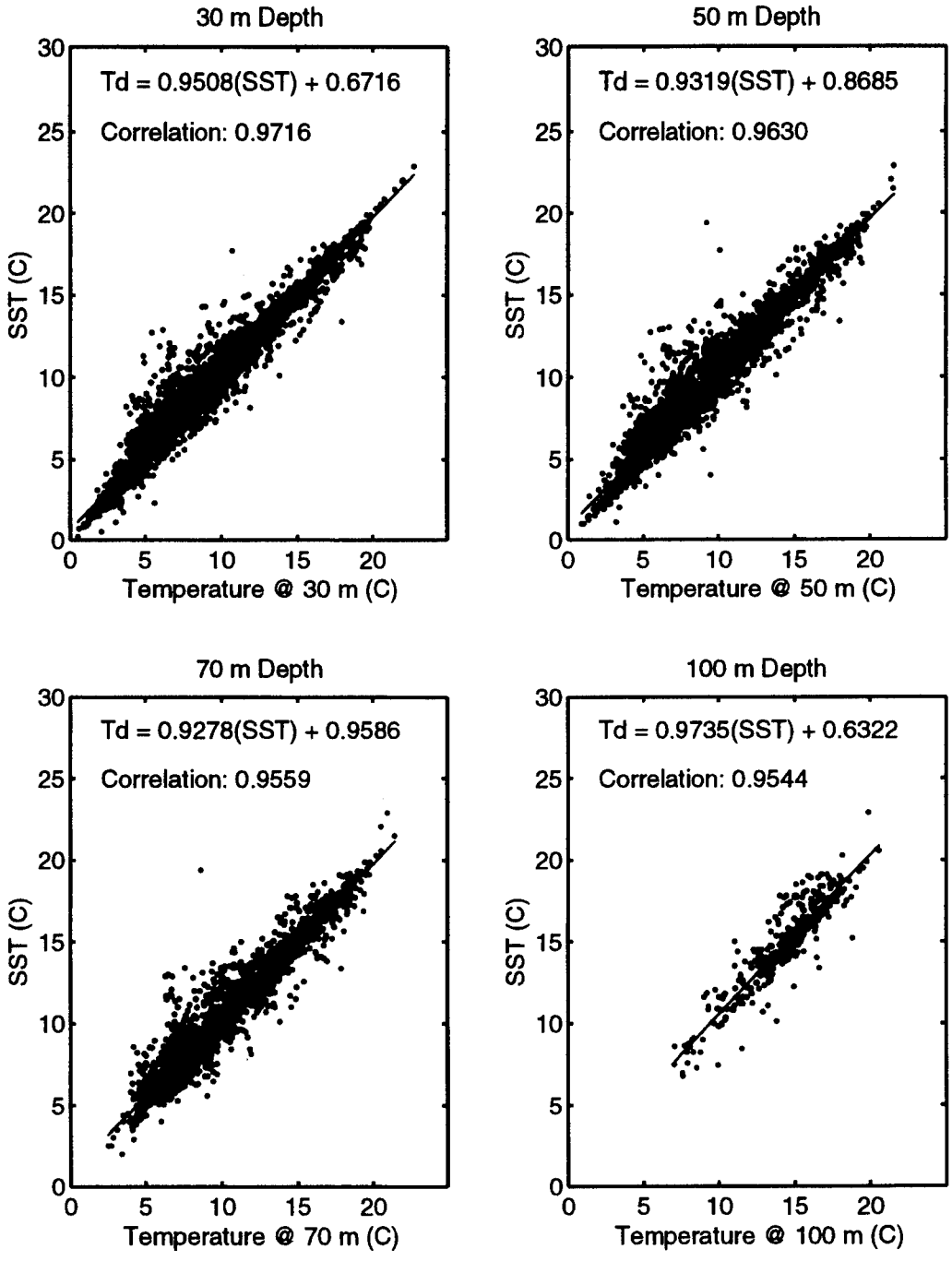

Figure 5.1. Winter regression analysis and correlation coefficients for SST versus temperature at 30, 50, 70 and 100 m. December through April are the "winter" months. In the regression equation, Td is the temperature at depth and SST is the sea surface temperature (°C).

Data Set	Slope	Intercept	Standard Error for Slope and Intercept	Upper and Lower 0.95 Confidence Limits	Number of Data Points
30 m	0.95075	0.63225	0.00344 0.03153	0.95750 0.94401 0.73344 0.69981	4527
50 m	0.93191	0.95857	0.00433 0.04107	0.94042 0.92340 0.94897 0.78794	3610
70 m	0.92778	0.86846	0.00638 0.06659	0.94030 0.91526 1.08910 0.82802	1996
100 m	0.97346	0.67163	0.02573 0.35129	1.02390 0.92300 1.32090 -0.05641	142

Table 5.1. A summary of the statistical data obtained during regression analyses for the winter months (December through April) in the Yellow Sea. Analyses performed at 30, 50, 70 and 100 m. A linear equation was produced and the slope and intercept values are listed. Additionally, the standard error and 95% upper and lower confidence level limits are provided. Intercept units are degrees centigrade (°C).

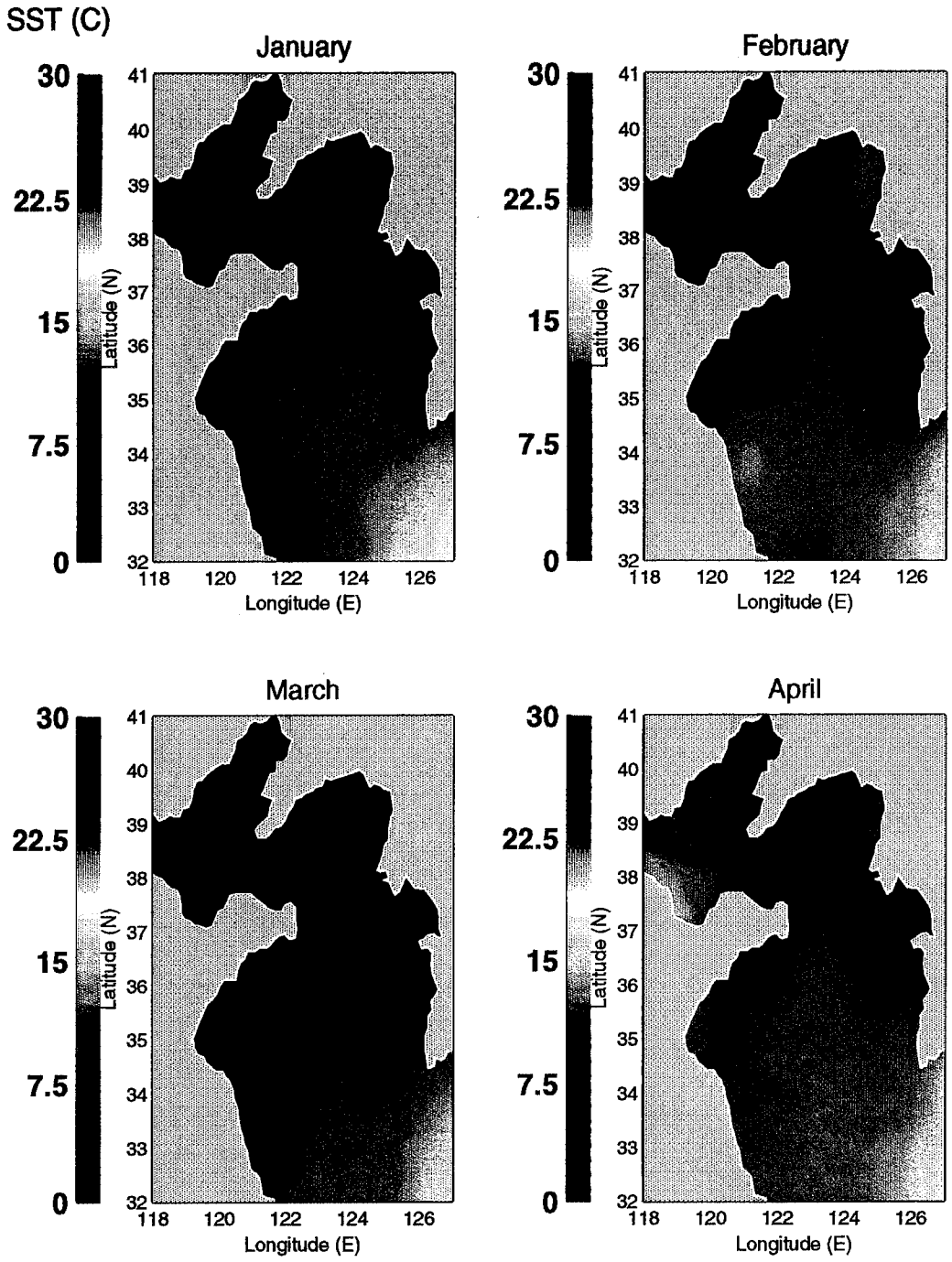

Figure 5.2a. Continuously shaded plots of sea surface temperature (SST) for the Yellow Sea for January, February, March and April. Data were obtained from the MOODS observational data base for the years 1929 to 1991. Temperatures are in °C.

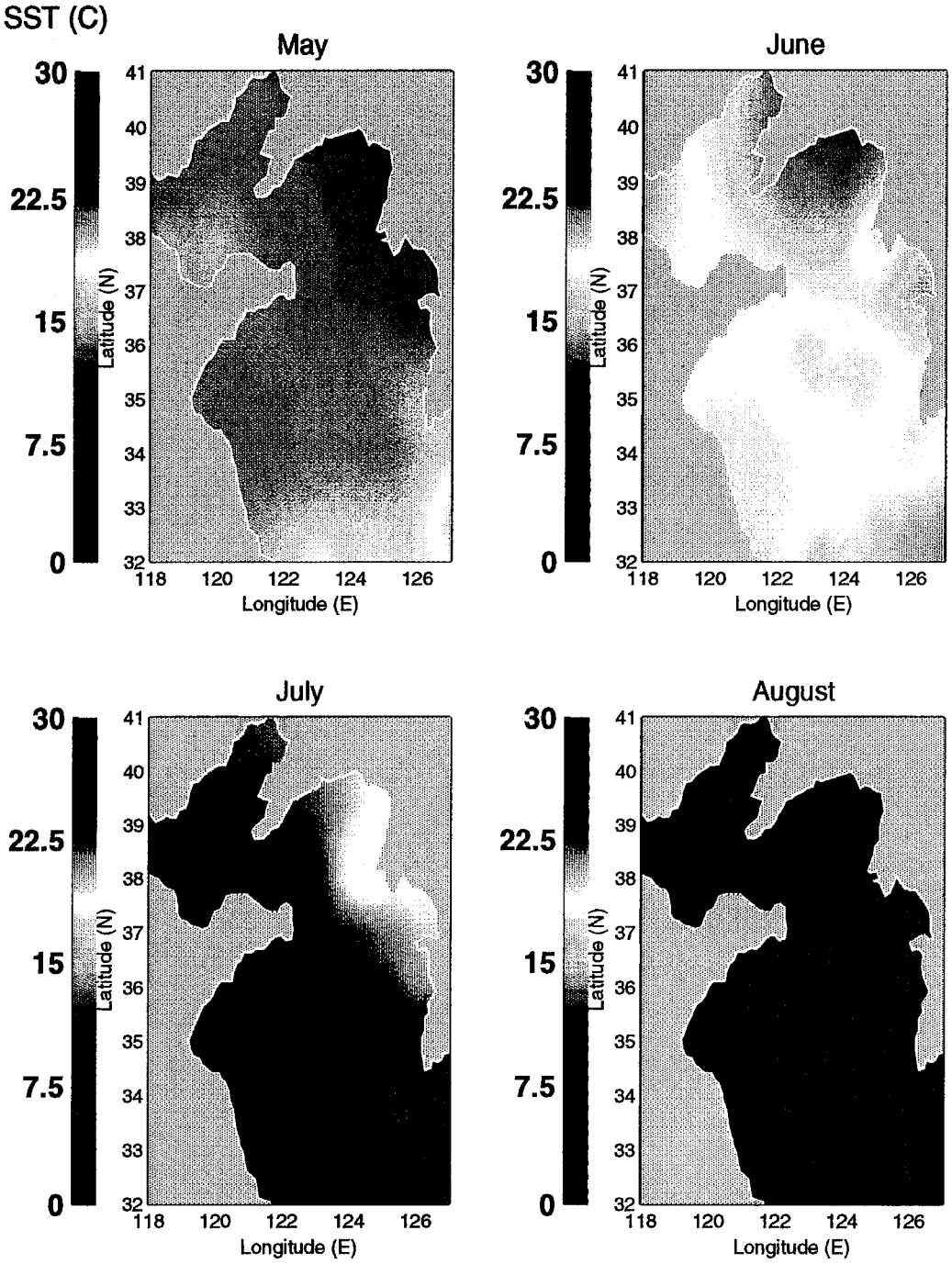

Figure 5.2b. Continuously shaded plots of sea surface temperature (SST) for the Yellow Sea for May, June, July and August. Data were obtained from the MOODS observational data base for the years 1929 to 1991. Temperatures are in °C.

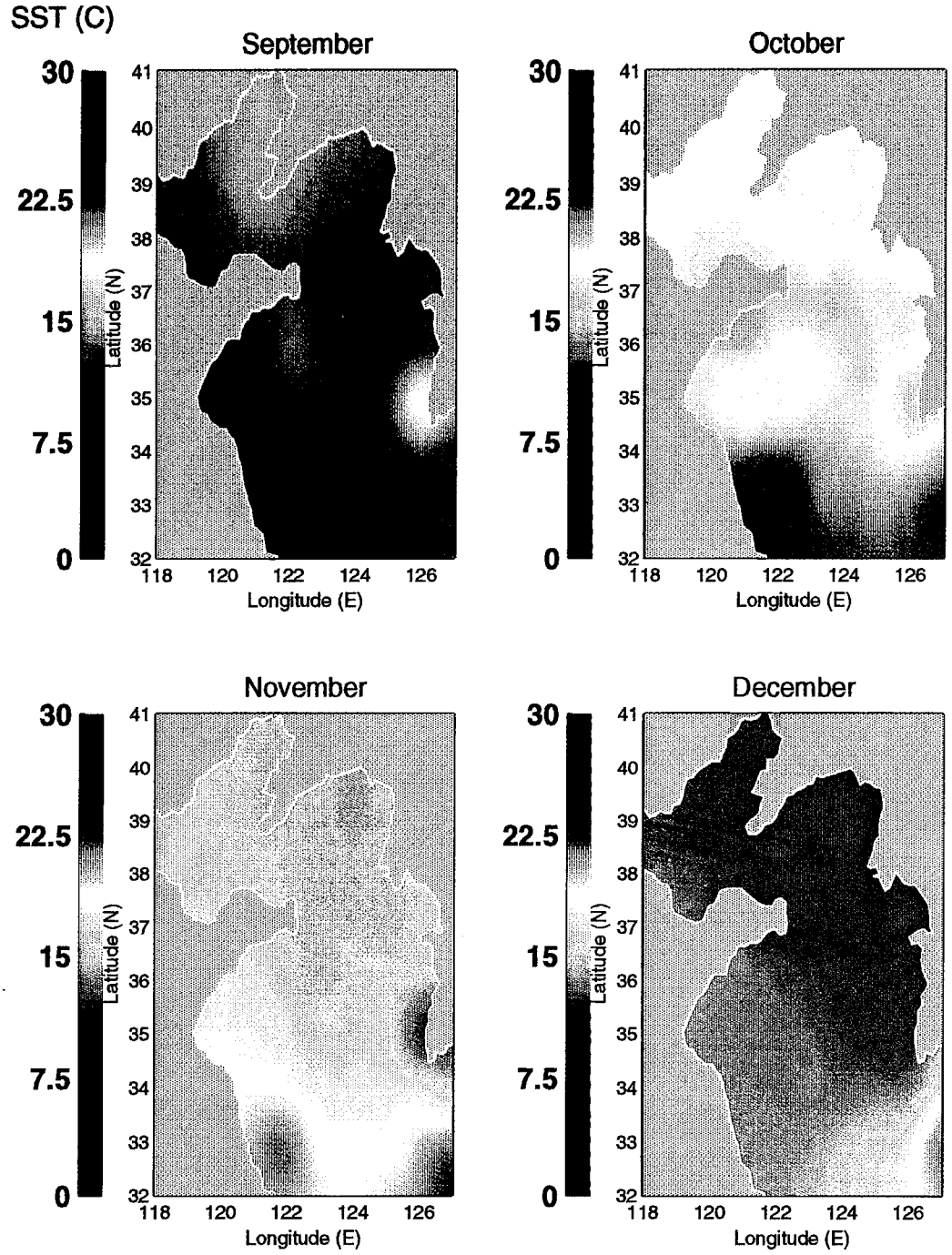

Figure 5.2c. Continuously shaded plots of sea surface temperature (SST) for the Yellow Sea for September, October, November and December. Data were obtained from the MOODS observational data base for the years 1929 to 1991. Temperatures are in °C.

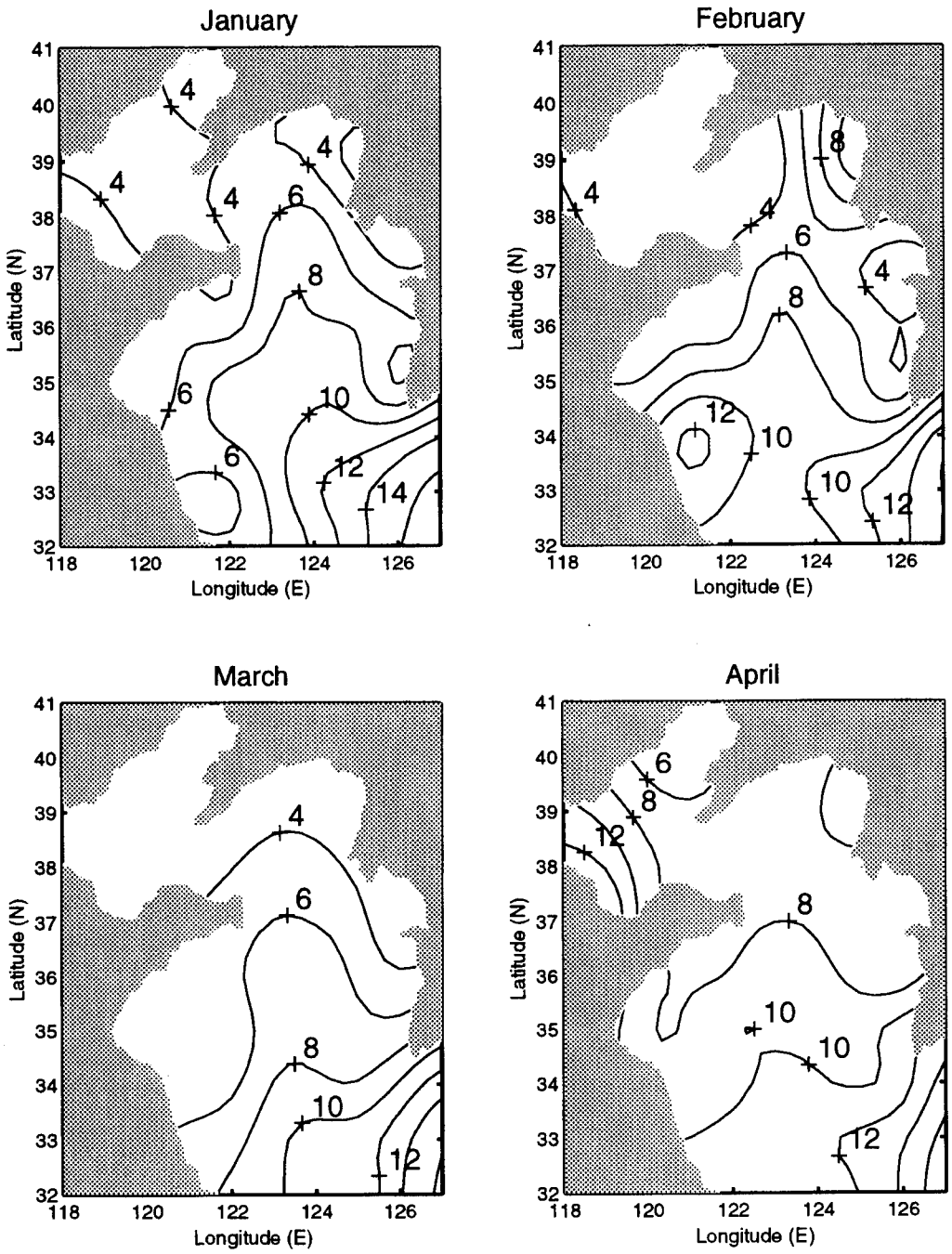

Figure 5.3a. Contour plots of SST in the Yellow Sea for January, February, March and April. Data were gridded and interpolated from the MOODS observational data set for the years 1929 to 1991. Temperatures in °C.

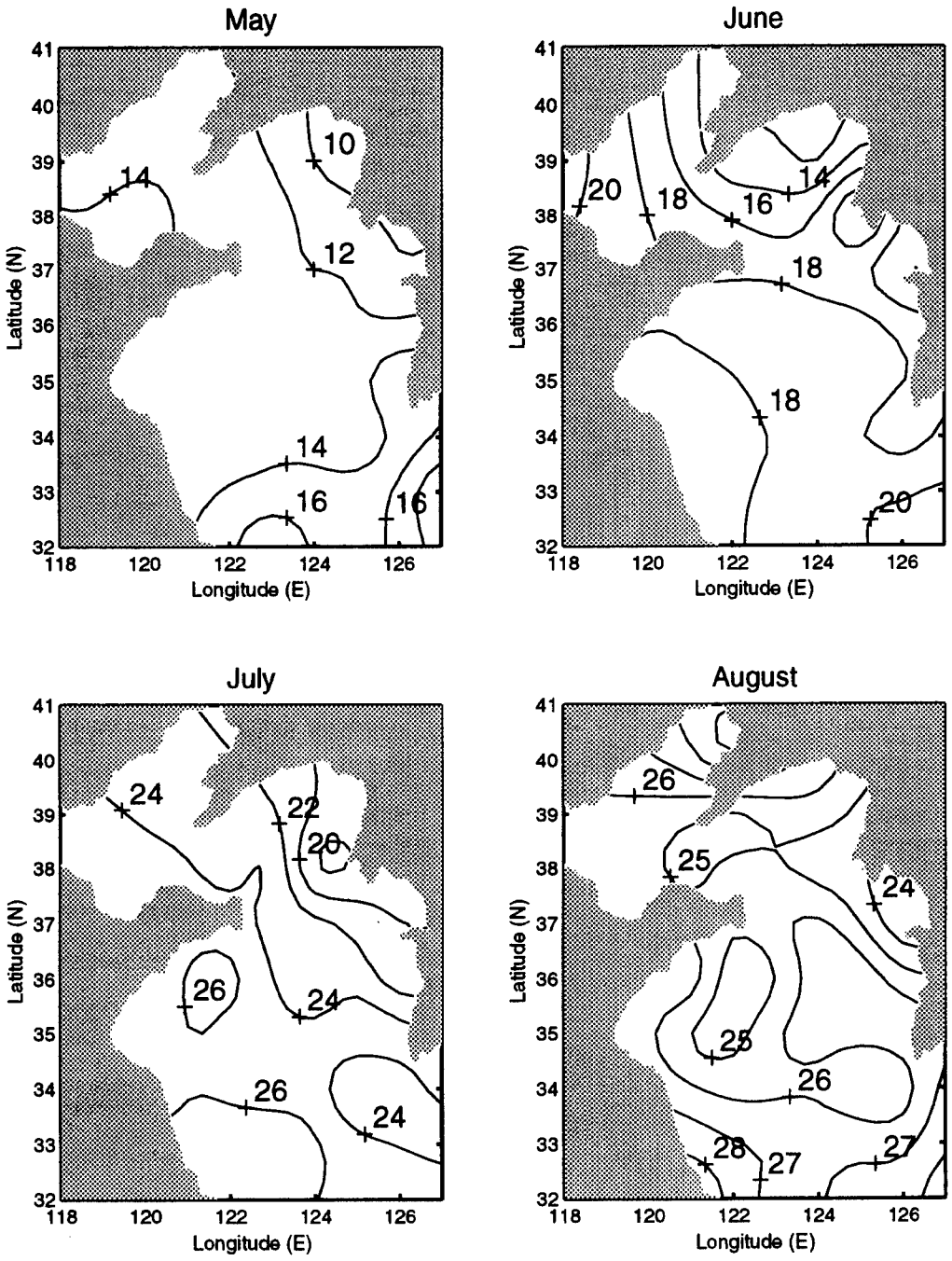

Figure 5.3b. Contour plots of SST in the Yellow Sea for May, June, July and August. Data were gridded and interpolated from the MOODS observational data set for the years 1929 to 1991. Temperatures in °C.

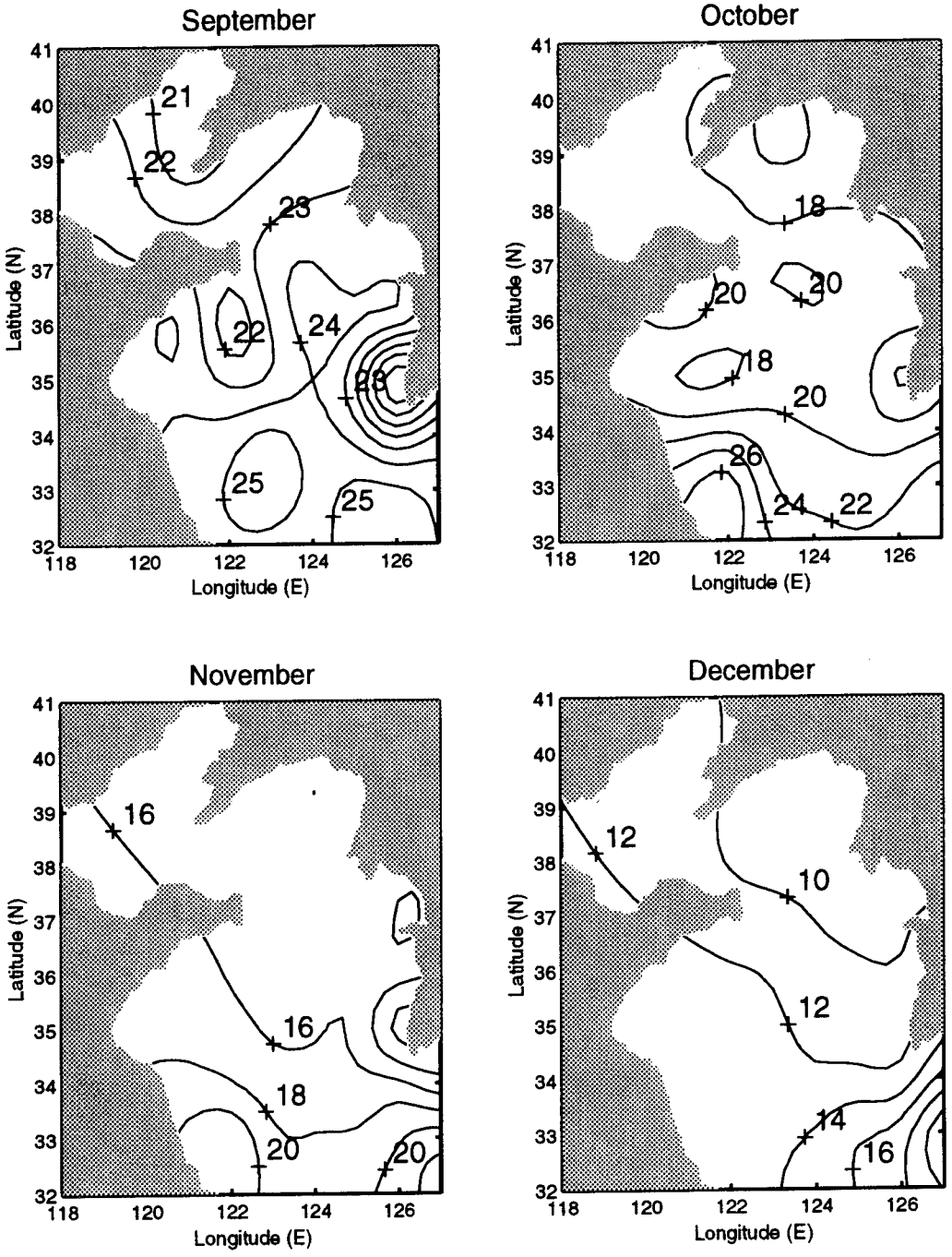

Figure 5.3c. Contour plots of SST in the Yellow Sea for September, October, November and December. Data were gridded and interpolated from the MOODS observational data set for the years 1929 to 1991. Temperatures in °C.

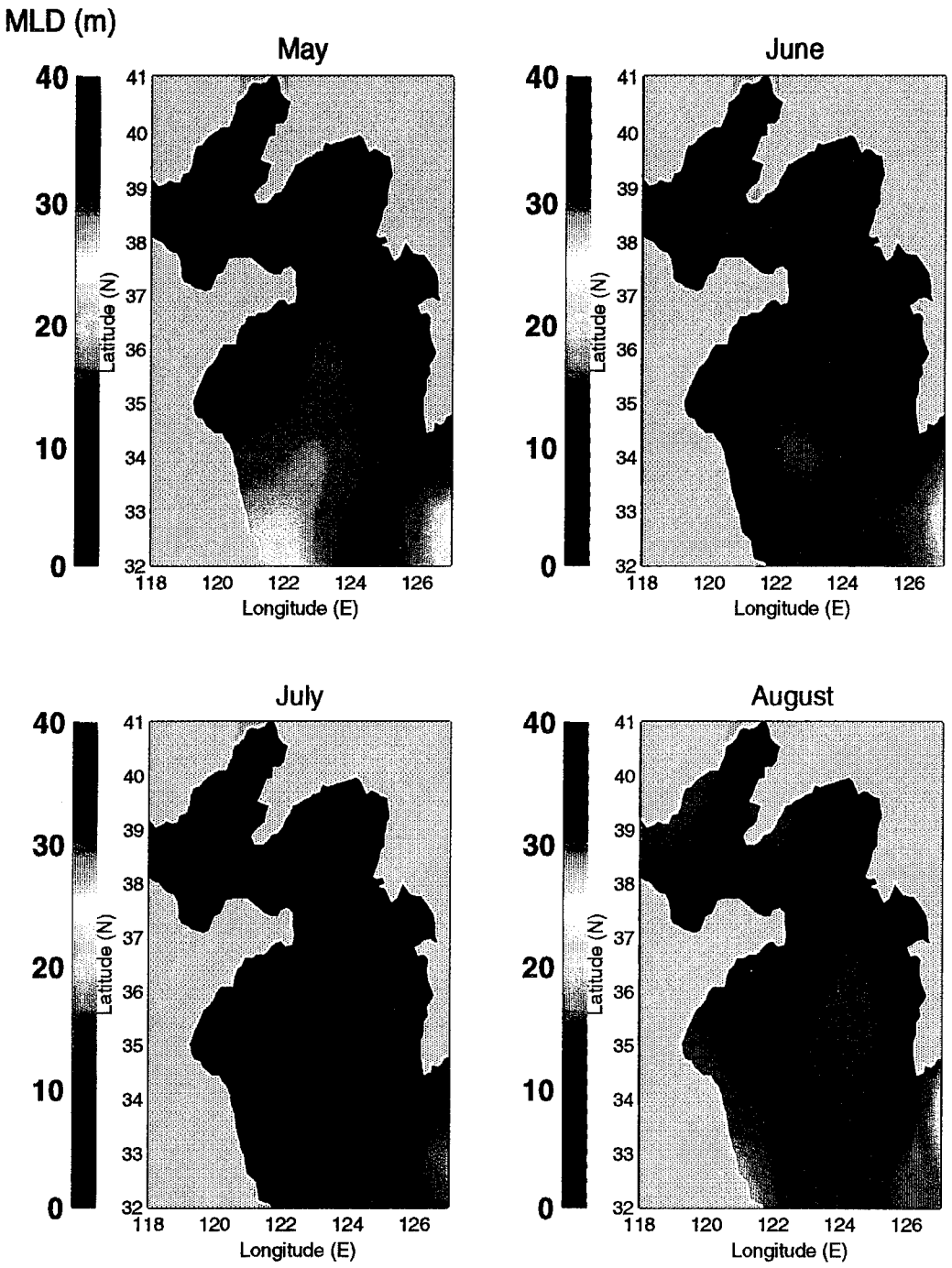

Figure 5.4a. Continuously shaded plots of mixed-layer depth (MLD) in the Yellow Sea for May (a transition month), June, July and August (summer months). Data were gridded and horizontally interpolated from the MOODS observational data base for the years 1929 to 1991. Depths are in meters (m).

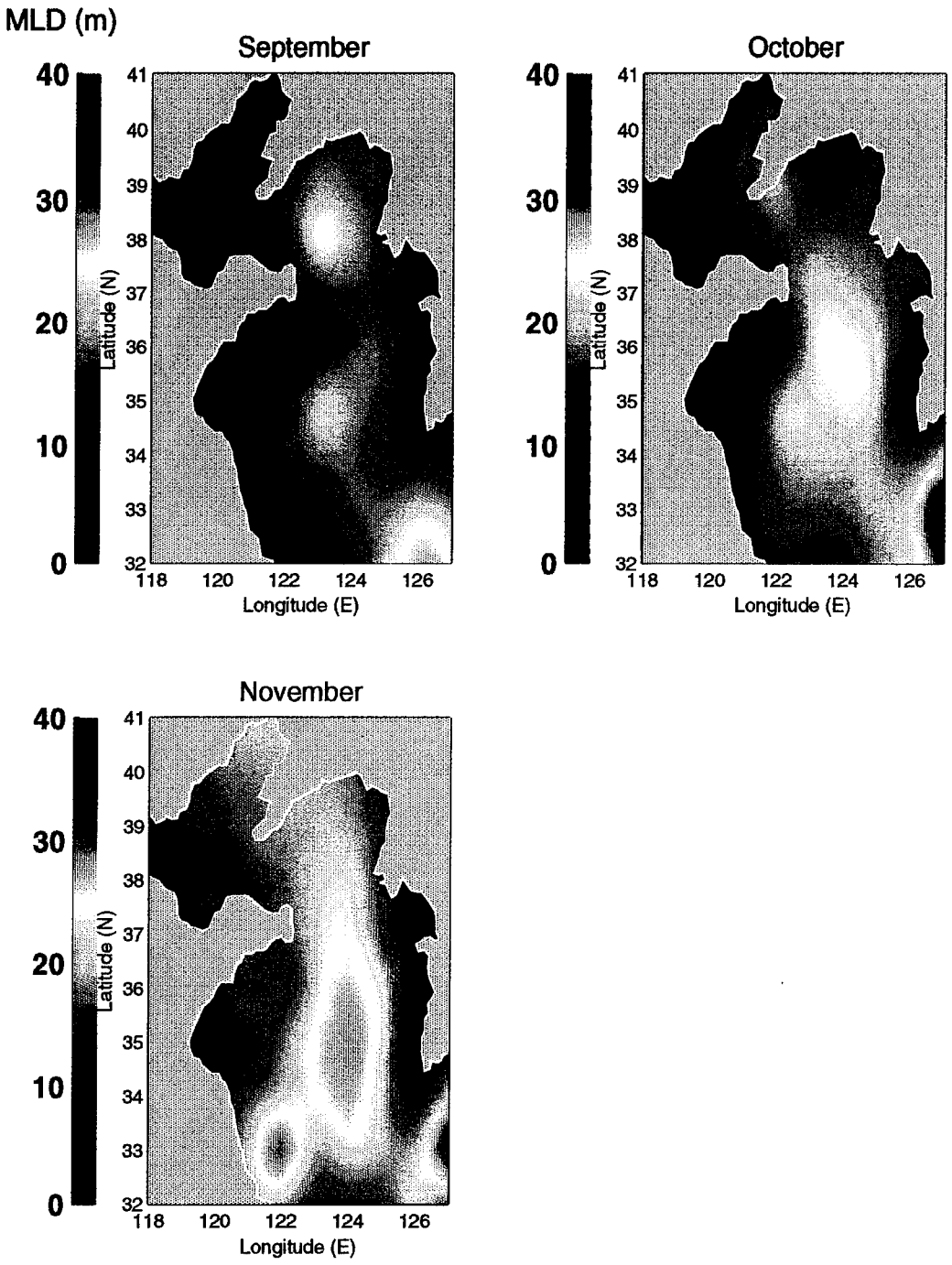

Figure 5.4b. Continuously shaded plots of mixed-layer depth (MLD) in the Yellow Sea for September, October (summer months) and November (a transition month). Data were gridded and horizontally interpolated from the MOODS observational data base for the years 1929 to 1991. Depths are in meters (m).

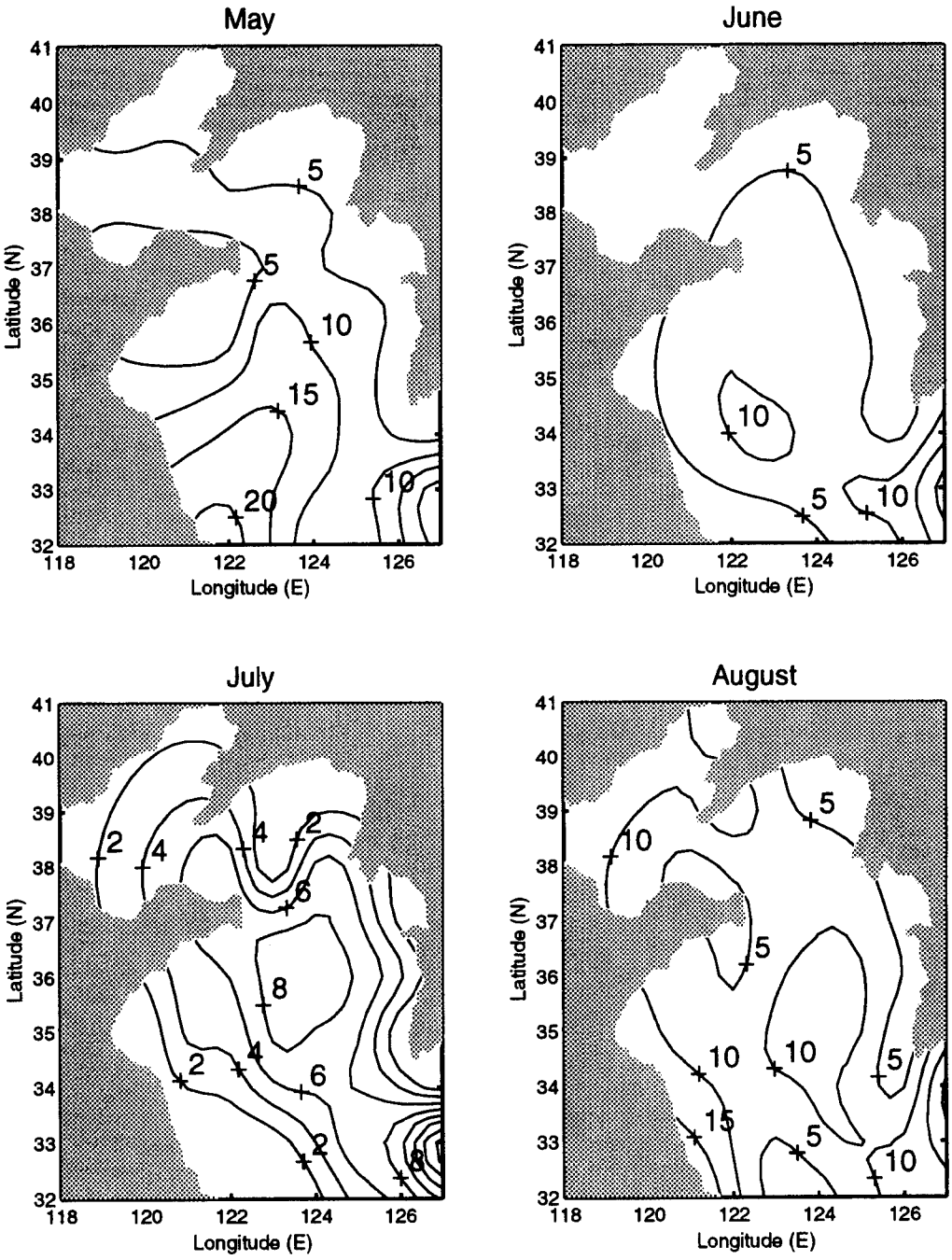

Figure 5.5a. Contour plots of mixed-layer depth (MLD) in the Yellow Sea for May (a transition month), June, July and August (summer months). Data were gridded and horizontally interpolated from the MOODS observational data base for the years 1929 to 1991. Depths are in meters (m).

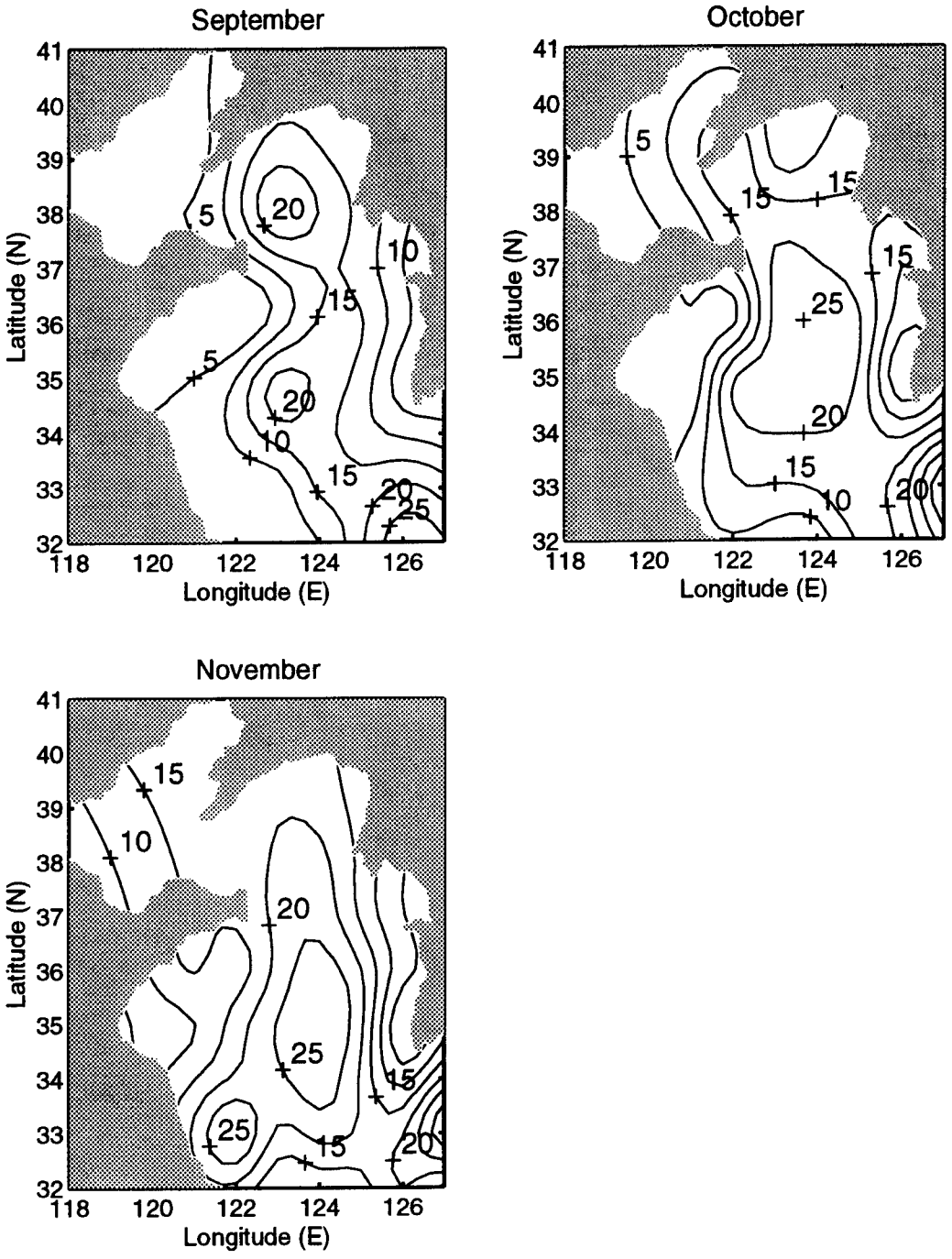

Figure 5.5b. Contour plots of mixed-layer depth (MLD) in the Yellow Sea for September, October (summer months) and November (a transition month). Data were gridded and horizontally interpolated from the MOODS observational data base for the years 1929 to 1991. Depths are in meters (m).

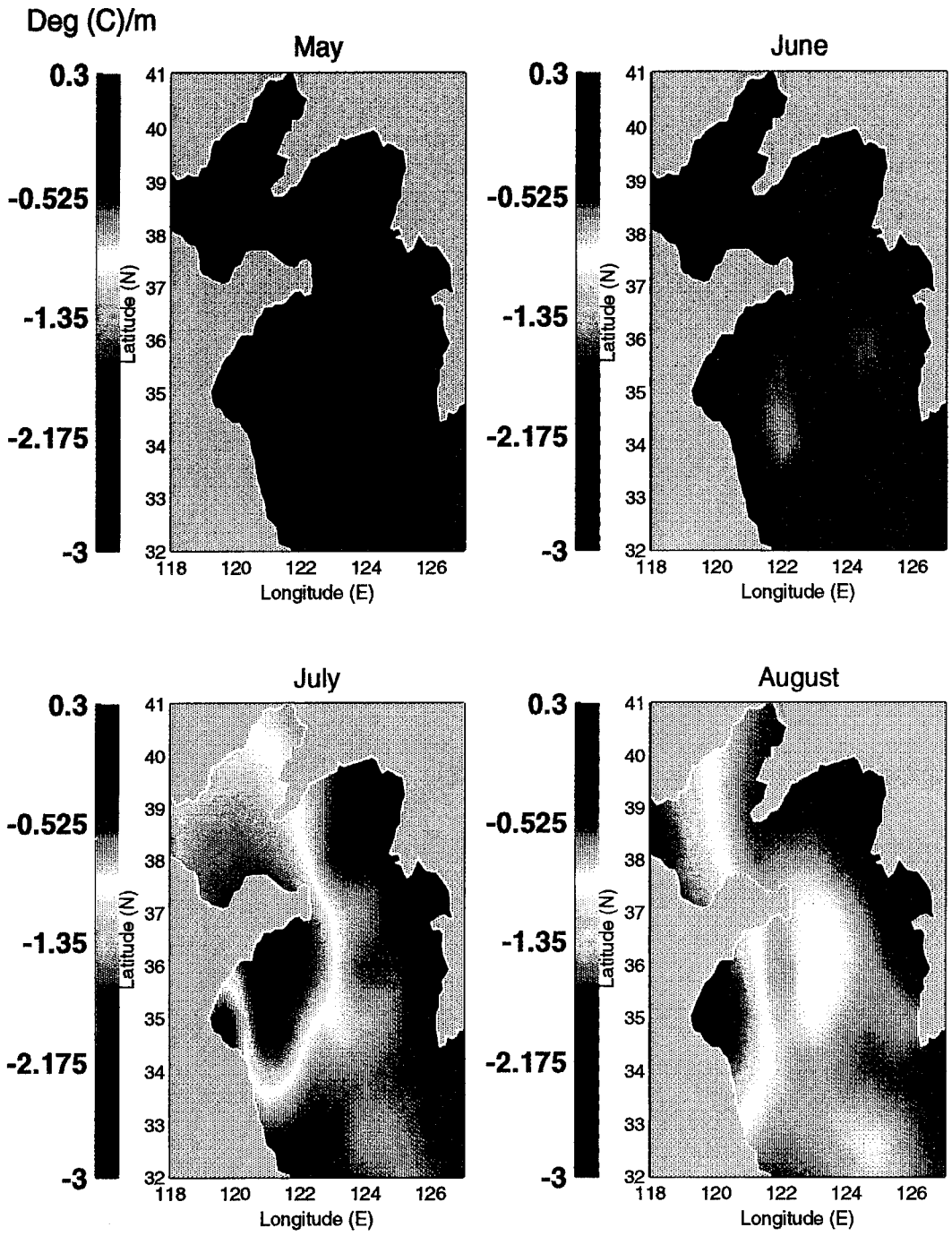

Figure 5.6a. Continuously shaded plots of the thermocline gradient in the Yellow Sea for May (a transition month), June, July and August (summer months). Data were produced by the Feature Model, gridded and horizontally interpolated. Model input data was the MOODS observational data base for the years 1929 to 1991. Gradient is in degrees centigrade per meter (°C/m).

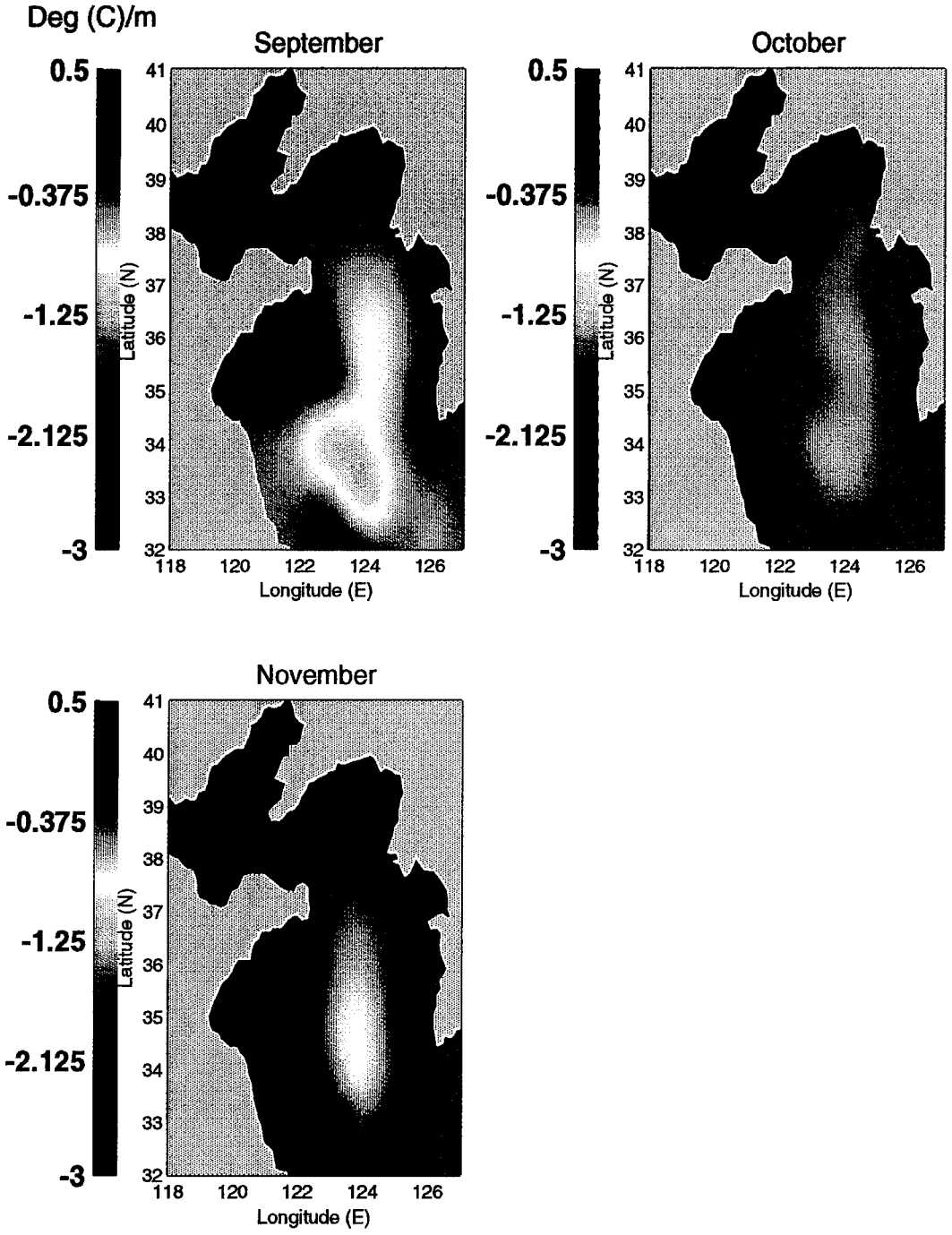

Figure 5.6b. Continuously shaded plots of the thermocline gradient in the Yellow Sea for September, October (summer months) and November (a transition month). Data were produced by the Feature Model, gridded and horizontally interpolated. Model input data was the MOODS observational data base for the years 1929 to 1991. Gradient is in degrees centigrade per meter (°C/m).

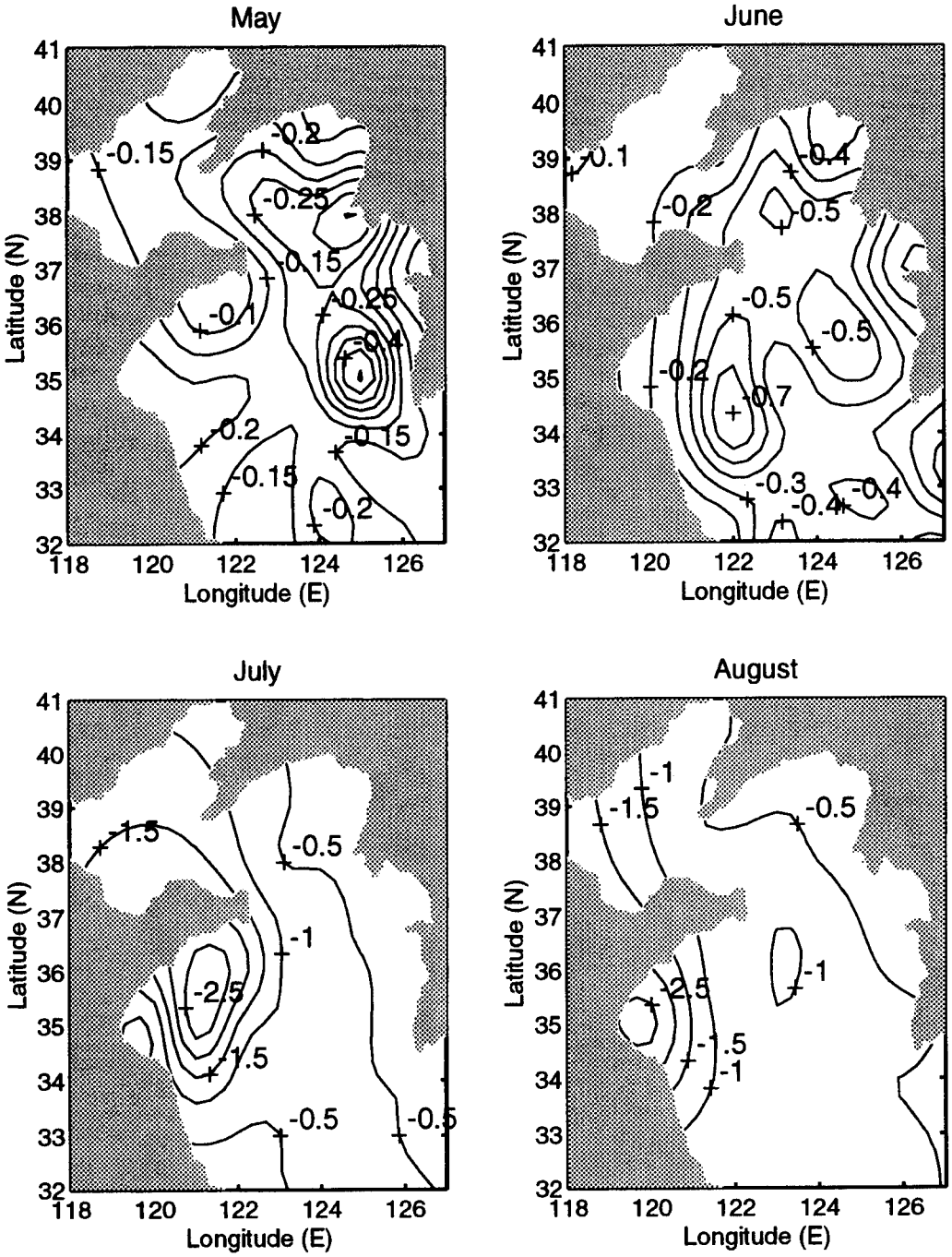

Figure 5.7a. Contour plots of the thermocline gradient in the Yellow Sea for May (a transition month), June, July and August (summer months). Data were produced by the Feature Model, gridded and horizontally interpolated. Model input data was the MOODS observational data base for the years 1929 to 1991. Gradient is in degrees centigrade per meter (°C/m).

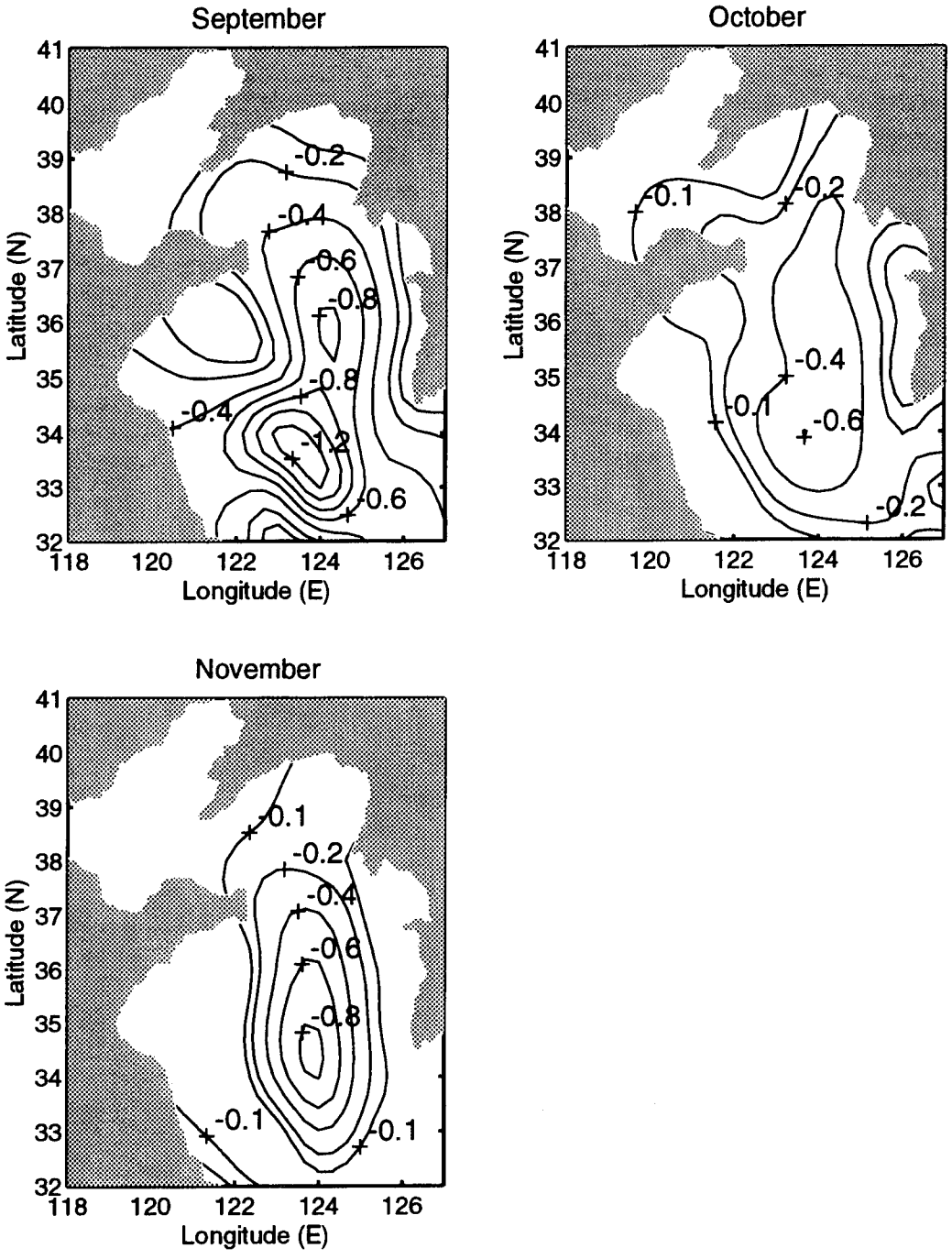

Figure 5.7b. Contour plots of the thermocline gradient in the Yellow Sea for September, October (summer months) and November (a transition month). Data were produced by the Feature Model, gridded and horizontally interpolated. Model input data was the MOODS observational data base for the years 1929 to 1991. Gradient is in degrees centigrade per meter (°C/m).

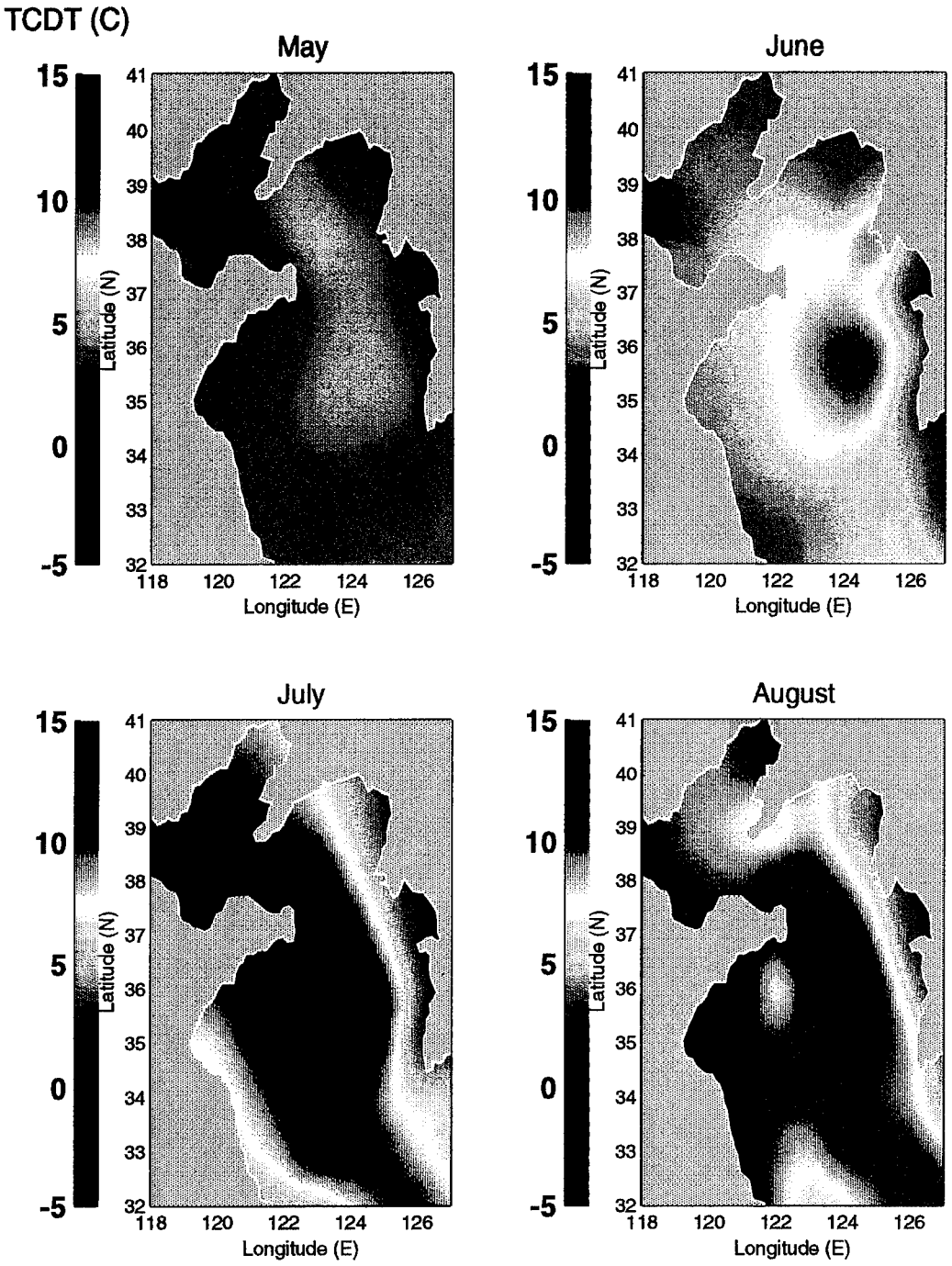

Figure 5.8a. Continuously shaded plots of the thermocline temperature difference (TCDT) in the Yellow Sea for May (a transition month), June, July and August (summer months). Data were produced by the Feature Model, gridded and horizontally interpolated. Model input data was the MOODS observational data base for the years 1929 to 1991. Temperature difference is in °C.

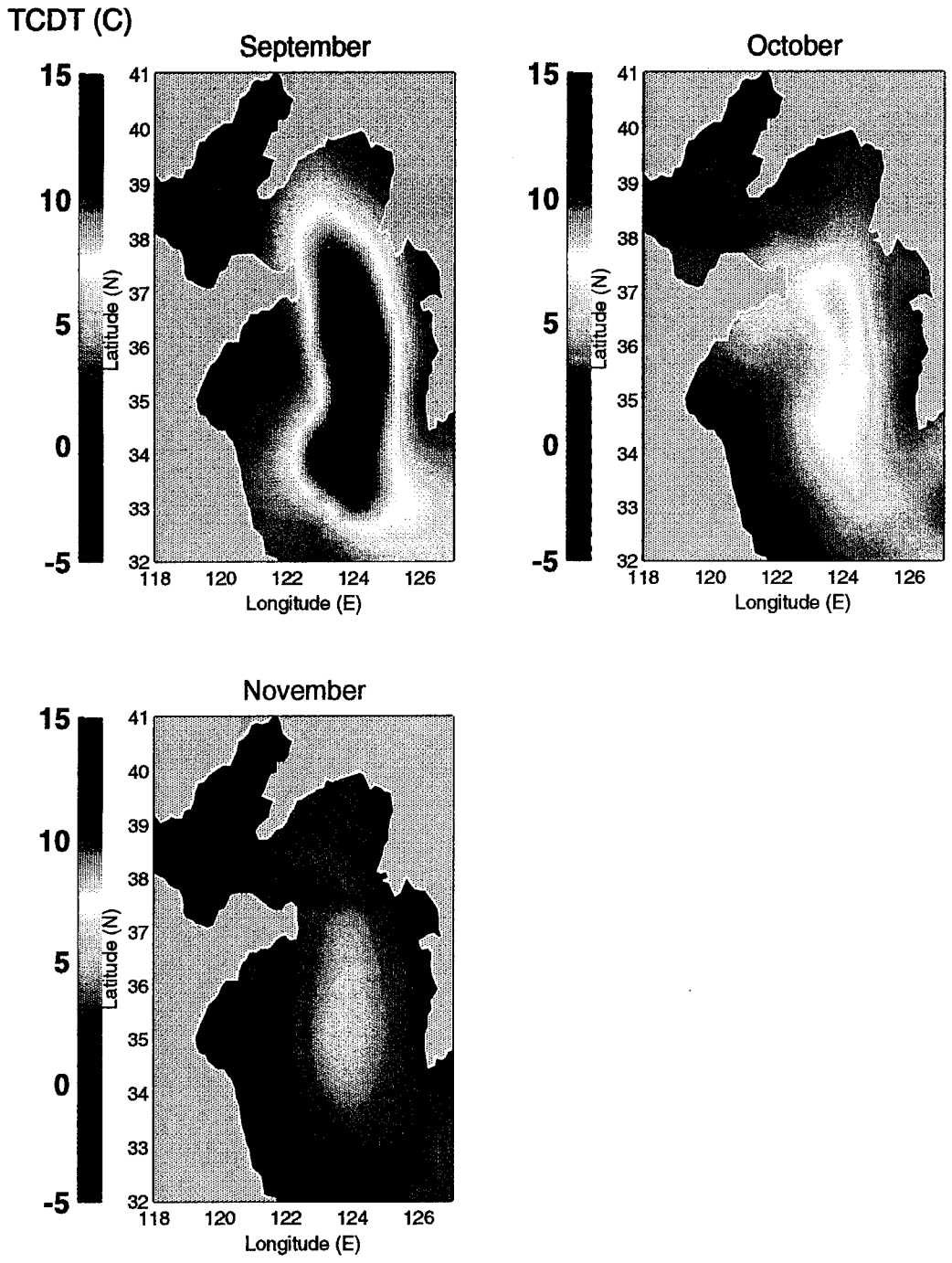

Figure 5.8b. Continuously shaded plots of the thermocline temperature difference (TCDT) in the Yellow Sea for September, October (summer months) and November (transition month). Data were produced by the Feature Model, gridded and horizontally interpolated. Model input data was the MOODS observational data base for the years 1929 to 1991. Temperature difference is in °C.

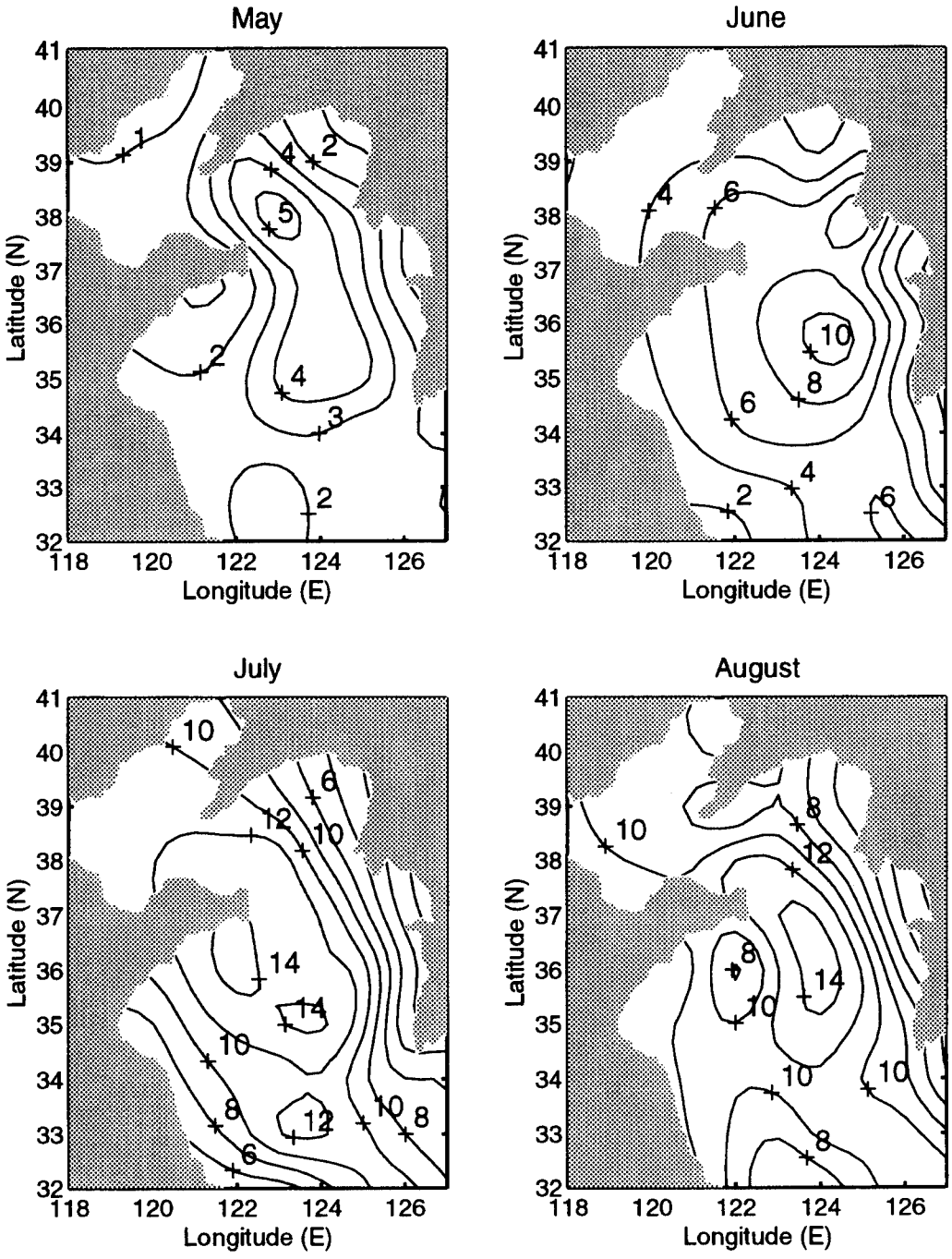

Figure 5.9a. Contour plots of the thermocline temperature difference (TCDT) in the Yellow Sea for May (transition month), June, July and August (summer months). Data were produced by the Feature Model, gridded and horizontally interpolated. Model input data was the MOODS observational data base for the years 1929 to 1991. Temperature difference is in °C.

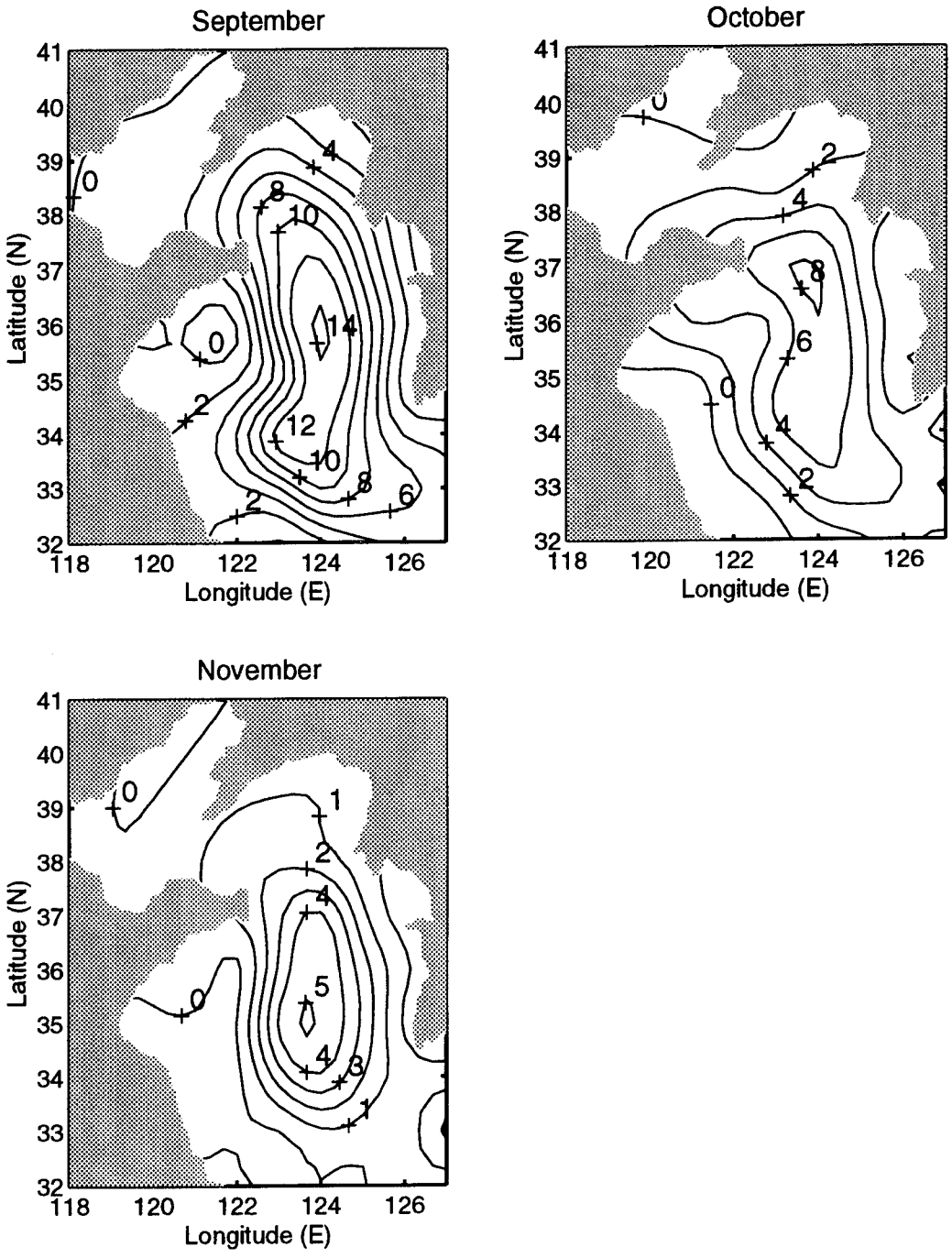

Figure 5.9b. Contour plots of the thermocline temperature difference (TCDT) in the Yellow Sea for September, October (summer months) and November (a transition month). Data were produced by the Feature Model, gridded and horizontally interpolated. Model input data was the MOODS observational data base for the years 1929 to 1991. Temperature difference is in °C.

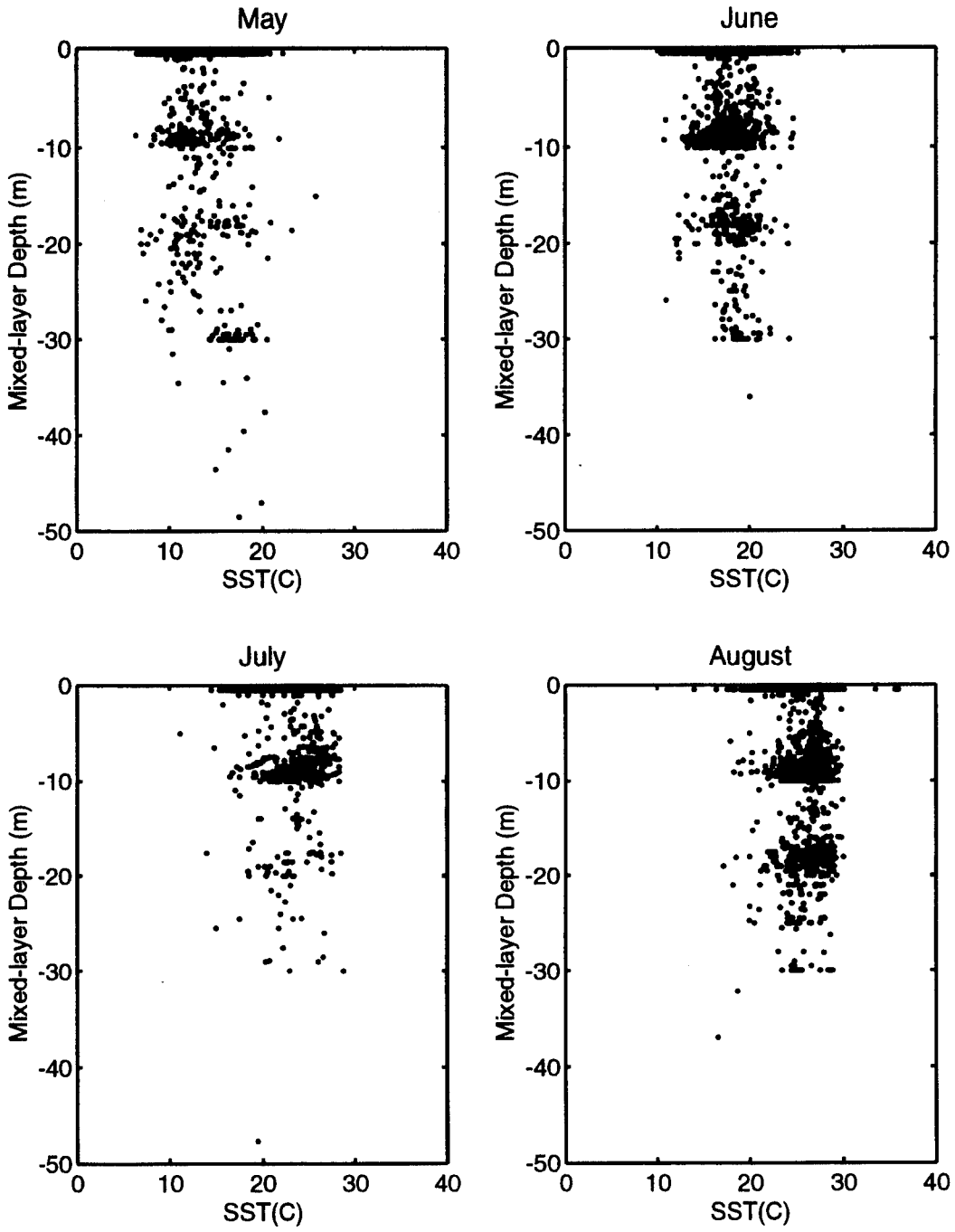

Figure 5.10a. Scatter plots of sea surface temperature (SST) versus mixed-layer depth (MLD) for May (a transition month), June, July and August (summer months). Data were produced by the Feature Model from MOODS observational data base profiles for the years 1929 to 1991. Depths are in meters (m) and temperatures in °C.

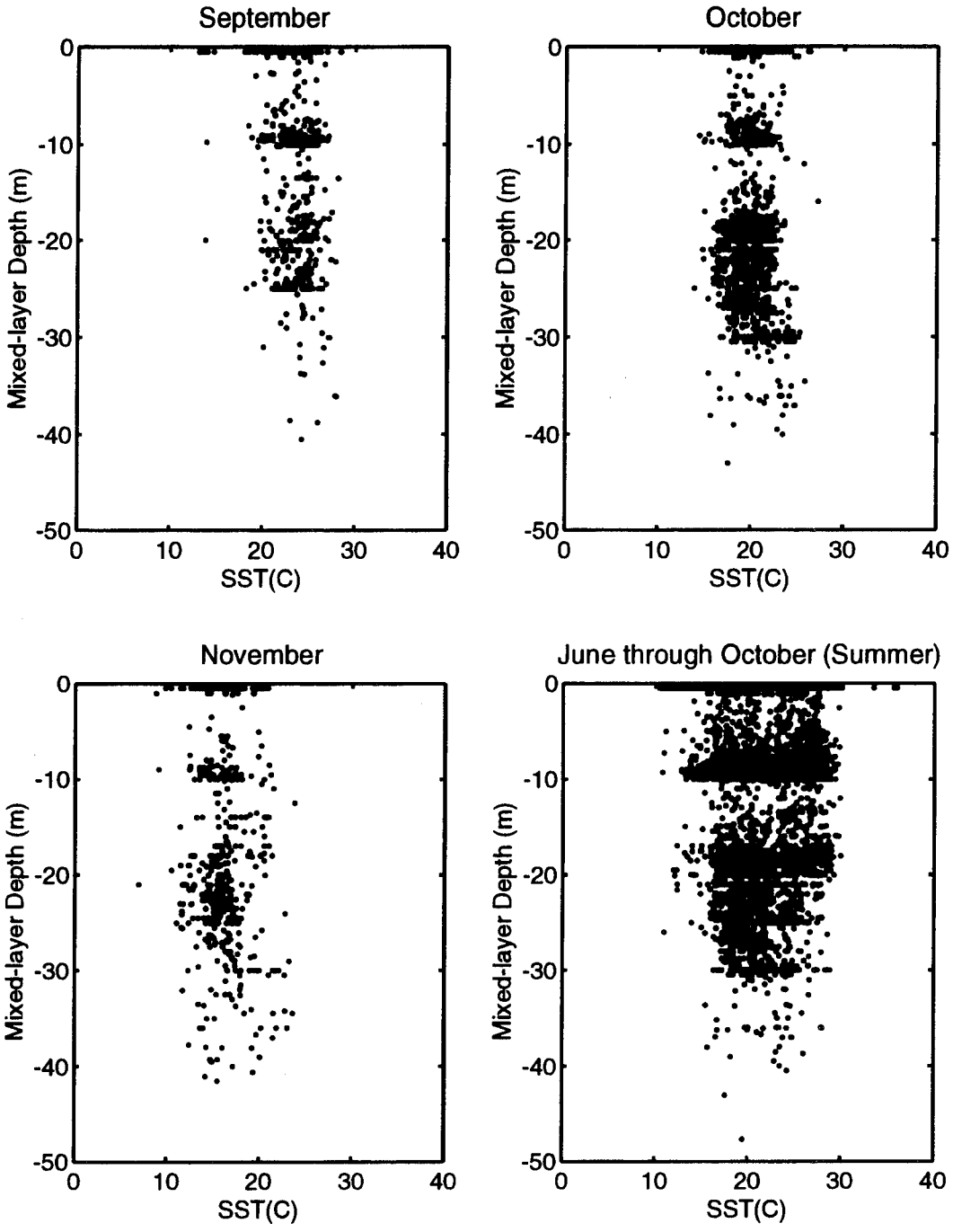

Figure 5.10b. Scatter plots of sea surface temperature (SST) versus mixed-layer depth (MLD) for September, October (summer months), November (a transition month) and all summer months combined. Data were produced by the Feature Model from MOODS observational data base profiles for the years 1929 to 1991. Depths are in meters (m) and temperatures in °C.

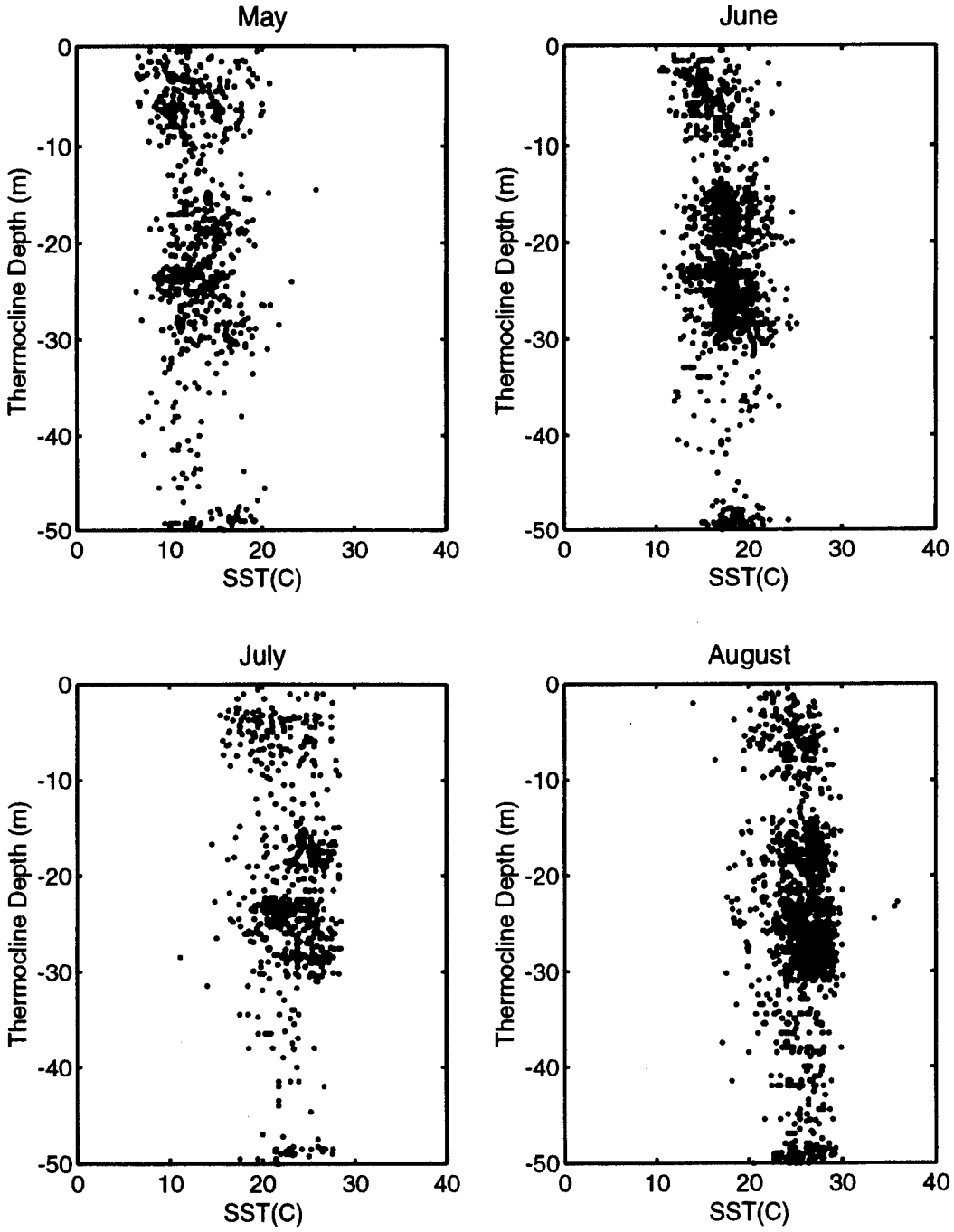

Figure 5.11a. Scatter plots of sea surface temperature (SST) versus thermocline depth for May (a transition month), June, July and August (summer months). Data were produced by the Feature Model from MOODS observational data base profiles for the years 1929 to 1991. Depths are in meters (m) and temperatures in °C.

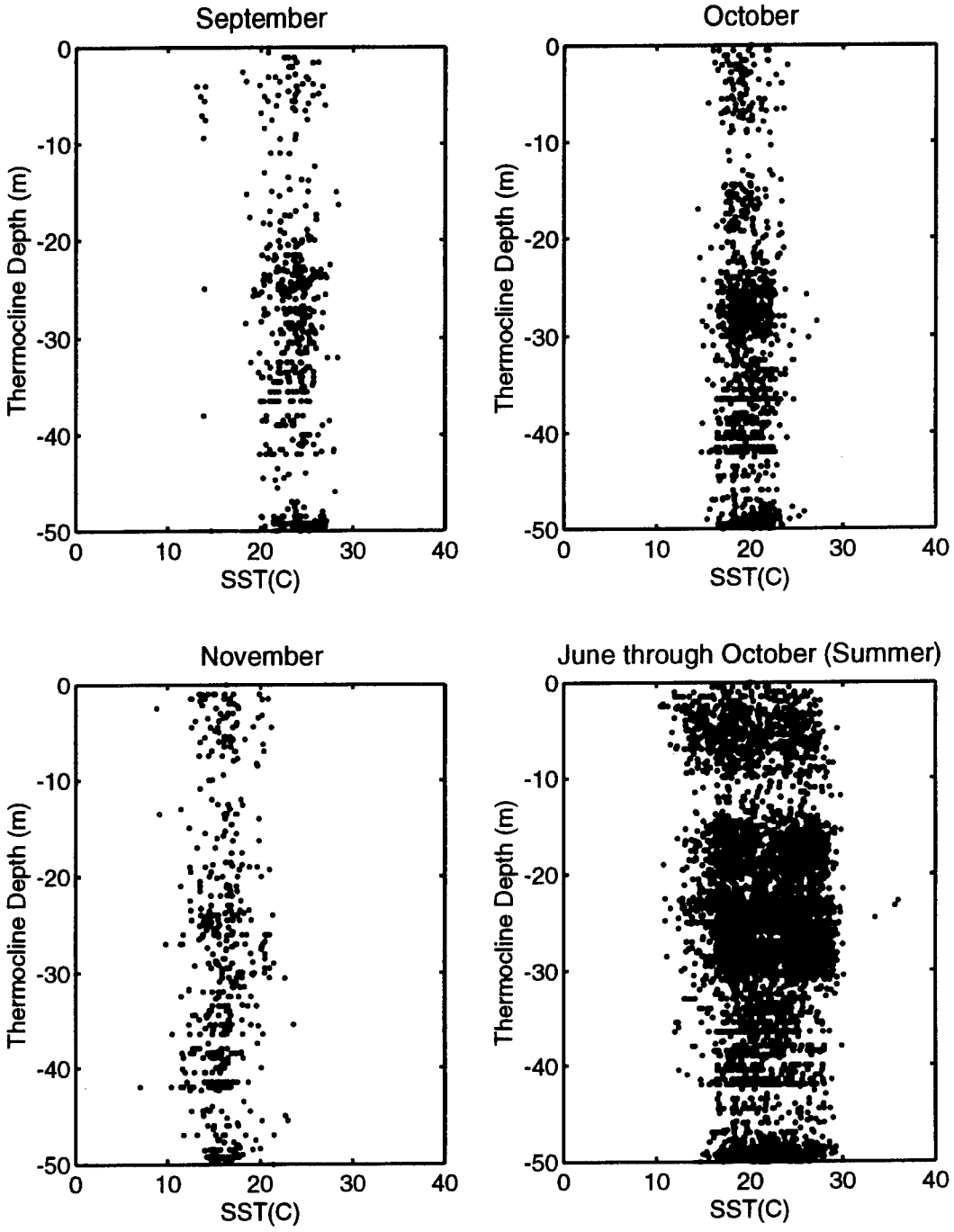

Figure 5.11b. Scatter plots of sea surface temperature (SST) versus thermocline depth for September, October (summer months), November (a transition month) and all summer months combined. Data were produced by the Feature Model from MOODS observational data base profiles for the years 1929 to 1991. Depths are in meters (m) and temperatures in °C.

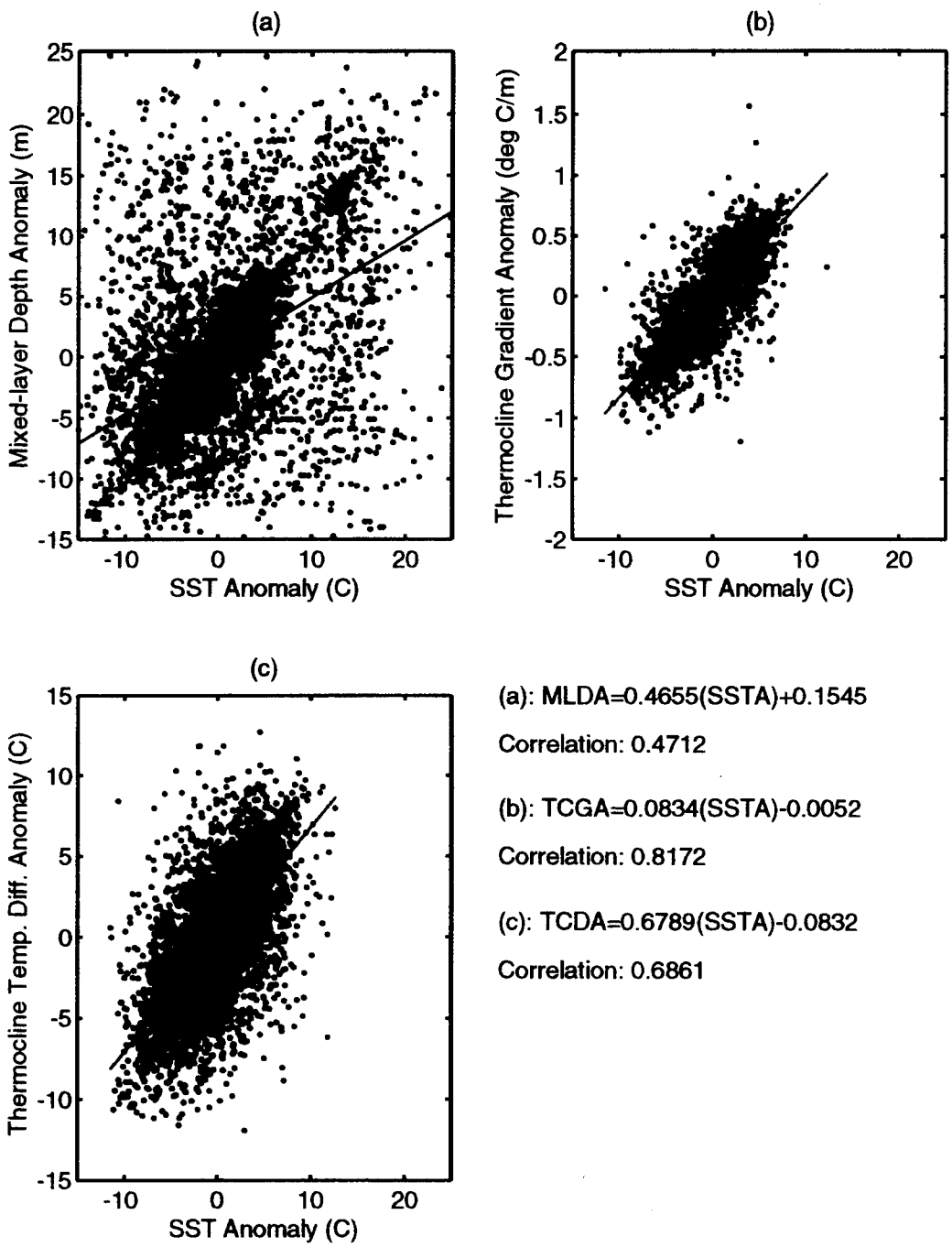

Figure 5.12. Scatter plots for the sea surface temperature anomaly (SSTA) versus the mixed-layer depth, thermocline gradient and thermocline temperature difference anomalies (MLDA, TCGA and TCDA). Data output from the Feature Model with input from the MOODS observational data base (1929 to 1991). Included are regression slopes, intercepts and correlation data. All summer months combined.

Data Set	Slope	Intercept	Standard Error for Slope and Intercept	Upper and Lower 0.95 Confidence Limits	Number of Data Points
SSTA vs MLDA	0.46553	0.15448	0.01192 0.08265	0.48889 0.44217 0.31651 -0.00755	5350
SSTA vs TCGA	0.08340	-0.00520	0.00773 0.00313	0.08480 0.08210 0.00010 -0.00480	5350
SSTA vs TCDA	0.67888	-0.08318	0.00984 0.03925	0.69817 0.65959 -0.00623 -0.16013	5350

Table 5.2. A summary of the statistical data obtained during regression analyses for the sea surface temperature anomaly (SSTA) versus the mixed-layer depth anomaly (MLDA), the thermocline gradient anomaly (TCGA) and the thermocline temperature difference anomaly (TCDA). A linear equation was produced and the slope and intercept values listed. Additionally, the standard error and 95% upper and lower confidence values are provided. The intercept units are meters (m), degrees centigrade per meter (°C/m) and degrees centigrade (°C) respectively.

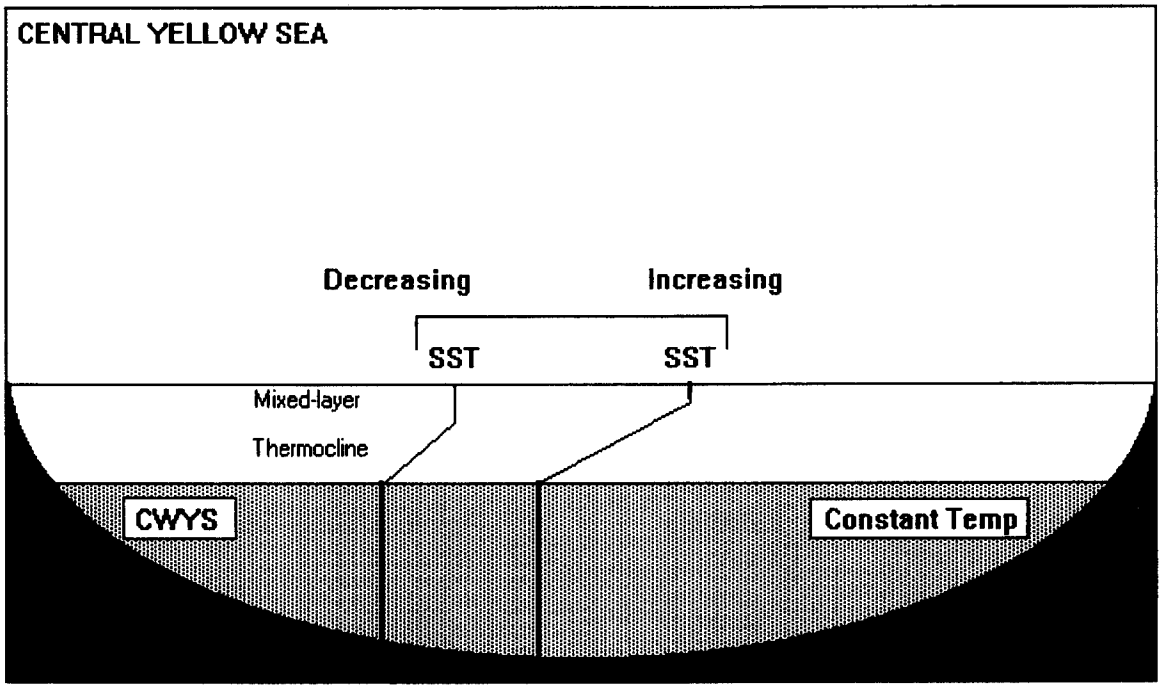

Figure 5.13. A depiction of the "anchoring" effect of the CWYS during the summer months in the Yellow Sea. As sea surface temperature (SST) increases, the base of the thermocline remains nearly constant, causing an increase in the thermocline gradient. As SST decreases, the difference in temperature between the SST and the deep layer decreases, reducing the thermocline gradient.

VI. CONCLUSION

The goal of our study was to construct a three-dimensional thermal structure of the Yellow Sea based primarily upon sea surface temperature. Ideally, we would be able to apply this technique to many areas using remotely sensed sea surface temperature rather than in-situ measurements. We applied a modeling approach to achieve our goal with a different model type applied to each of two profile types dominant in the Yellow Sea. These profile types were season-specific and due to entirely different forcing mechanisms.

Our data set was composed of approximately 15,000 observed profiles from the MOODS worldwide observational data base. The observations spanned the years 1929 to 1991 and were sourced from all common instrument types. Due to a sparsity of data for individual years, monthly bins were constructed using all years.

The winter season, with cold air temperatures and stronger winds, displayed nearly isothermal vertical structure as a result of strong mixing. The resulting one-layer, well-mixed vertical profiles were depicted by regression analysis between sea surface temperature and subsurface temperature. We achieved very good results with slopes of the regressions greater than 0.92 for SST versus the temperature at 30, 50, 70 and 100 m. Correlation coefficients were all greater than 0.95, indicating good coherence. The lack of a true isothermal relationship in our results is owed to interannual variability introduced by the monthly binning process, calibration errors of sampling equipment and analyst errors.

The summer season is characterized by strong surface heating, weaker winds and a resulting multi-layered vertical structure. This layered structure consists of the mixed-layer, thermocline and deep layer. In order to extract depth and temperature gradient information about these features, a physically-based "Feature Model" was employed. This approach involved the fitting of a "first guess" characteristic file to a vertically interpolated, high-resolution "gradient space" transformation of each observed profile. The fitted "first guess" file thus produced a modeled profile from which characteristics could be extracted in the form of inflection point depths and layer gradients. To ensure quality data, RMS error calculations were performed on each characteristic and gradient, compared to a standard, and either accepted or rejected. The resulting accepted data were analyzed both in total quantity form (mean plus perturbation) and as perturbations alone. Ultimately we used the perturbation data as a base for our analyses.

We performed statistical analysis on three perturbation characteristic pairs: SST anomaly versus mixed-layer depth anomaly, SST anomaly versus thermocline gradient anomaly and SST anomaly versus thermocline temperature difference anomaly. The mixed-layer depth anomaly analysis produced mediocre results with correlation values of less than 0.5. The slope and intercept of the regression analysis were also poor. The thermocline gradient anomaly comparison was much better with a correlation of 0.82 and a regression slope of 0.82. Comparison of the thermocline temperature difference anomaly was also mediocre with a correlation of 0.69 and regression slope of 0.68.

We attributed our mixed results to a few key factors. The data set quality was questionable, as witnessed by sampling errors we discovered. These errors were present only in lower resolution observations. When CTD data were used exclusively, these errors vanished. The introduction of interannual variability into our data set by compositing all years together may have negatively affected our results. Finally, interpolation techniques used to produce a gridded Yellow Sea data set may have introduced errors in data-sparse regions.

These problems were a result of data quality issues and not the analysis techniques we applied. We feel that our modeling approach was robust and flexible and could applied to many regions with good results, provided a good data source is available. Our results indicate that data quality is critical to the successful employment of these techniques and should be the prime consideration in future applications.

LIST OF REFERENCES

Wan, B.J., Guo, B.H. and Chen, Z.S., A three-layer model for the thermal structure in the Huanghai Sea, *Acta Oceanologica Sinica*, 9(2),159-172, 1990.

Zhao, B.R., Basic characteristics and forming mechanism of the sharp thermocline in the Bohai Sea, Huanghai Sea and northern East China Sea, *Acta Oceanologica Sinica*, 8(4), 497-510, 1989.

Boyle, J.S. and Chen, T.-J., Synoptic aspects of the wintertime East Asian monsoon, in *Monsoon Meteorology*, chap. 2, sect. 5, edited by C.P. Chang and T.N. Krishnamurti, pp. 125-160, Oxford Press, New York, 1987.

Chu, P.C., Garwood, R.W. and Muller, P., Unstable and damped modes in coupled ocean mixed layer and cloud models, *Journal of Marine Systems*, 1(1), 1-11, 1990.

Chu, P.C. and Garwood, R.W., On the two-phase thermodynamics of the couple cloud-ocean mixed layer, *Journal of Geophysical Research*, 96, 3425-3436, 1991.

Elms, J.D., U.S. Navy regional climatic study of the central east Asian coast and associated waters, U.S. Naval Oceanography Command report NAVAIR 50-1C-556, 1990.

Guan, B., Patterns and structures of the currents in Bohai, Huanghai and East China Seas, in *Oceanology of China Seas*, edited by Y. Liang and C.K. Tseng, pp. 17-26, Kluwer, Boston, 1994.

Haeger, S.D., A gradient model for the Bering Sea temperature structure, U.S. Naval Oceanography Command Technical Report, in press.

Krishnamurti, T.N. and Surti, N., Observational aspects of summer monsoon, in *Monsoon Meteorology*, chap. 1, sect. 1, edited by C.P. Chang and T.N. Krishnamurti, pp. 3-25, Oxford Press, New York, 1987.

Langhill, R.H., Forecasting guide for the Republic of Korea, Det. 18, 20th Weather Squadron, 1st Weather Wing, USAF, 1976.

Li, H. and Yuan, Y., On the formation and maintenance mechanisms of the cold water mass of the Yellow Sea, *Chin. J. Oceanol. Limnol.*, 10(2), 97-106, 1992.

Jin, M.B., Wang, Z.S. and Xu, B.C., Three-dimensional numerical prediction of vertical temperature structure of the Huanghai and the Bohai Seas, *Acta Oceanologica Sinica*, 12(4), 511-520, 1993.

Nestor, M.J.R., The environment of South Korea and adjacent sea areas, U.S. Naval Environmental Prediction Research Facility Technical Report No. TR 77-03, Monterey, CA, 1977.

Liu, S.X., Shen, Y.Q., Wang, Y.Q. and Han, S.X., Preliminary analysis of distribution and variation of perennial monthly mean water masses in the Bohai Sea, the Huanghai Sea and the East China Sea, *Acta Oceanologica Sinica*, 11(4), 483-498, 1992.

Su, Y. and Weng, X., Water masses in China Seas, in *Oceanology of China Seas*, edited by Y. Liang and C.K. Tseng, pp. 3-16, Kluwer, Boston, 1994.

Turner, J.S. and Kraus, E.B., A one-dimensional model of the seasonal thermocline, *Tellus*, 19, 88-97, 1967.

Watts, I.E.M., Climates of China and Korea, in *World Survey of Climatology*, vol. 8, edited by H. Arakawa, pp.1-117, Elsevier, New York, 1969.

Yanagi, T. and Takahashi, S., Seasonal variation of circulations in the East China Sea and the Yellow Sea, *Journal of Oceanography*, 49, 503-520, 1993.

INITIAL DISTRIBUTION LIST

		No. Copies
1.	Defense Technical Information Center Cameron Station Alexandria, VA 22304-6145	2
2.	Librarian, Code 52 Naval Postgraduate School 411 Dyer Rd. Rm 252 Monterey, CA 93943-5114	2
3.	Superintendent Attn: Chairman, Department of Meteorology (Code MR/HY) Naval Postgraduate School Monterey, CA 93943-5000	1
4.	Superintendent Attn: Chairman, Department of Oceanography (Code OC/CO) Naval Postgraduate School Monterey, CA 93943-5000	1
5.	Superintendent Attn: Professor Peter C. Chu Naval Postgraduate School Monterey, CA 93943-5000	3
6.	Lieutenant Charles R. Fralick, Jr. 3824 Larchwood Dr. Virginia Beach, VA 23456	2
7.	Superintendent Naval Research Laboratory 7 Grace Hopper Avenue Stop 2 Monterey, CA 93943-5502	1
8.	Chairman Oceanography Department U.S. Naval Academy Annapolis, MD 21402	1
9.	Office of Naval Research (Code 420) 800 N. Quincy Street Arlington, VA 22217	1
10.	Library Scripps Institution of Oceanography P.O. Box 2367 La Jolla, CA 92037	1

11. Dr. Mike Carron 1
Naval Oceanographic Office, Code N3T
Stennis Space Center, MS 39522

12. Steven D. Haeger 2
Naval Oceanographic Office, Code N3T
Stennis Space Center, MS 39522

13. NOAA Library 1
7600 Sand Point Way NE
Building 3
Seattle, WA 98115

14. CDR David Martin 1
Naval Oceanographic Office. Code N22
Stennis Space Center, MS 39522